Visualizing patterns of gene expression in growing Bacillus subtilis biofilms

Visualizing patterns of gene expression in growing Bacillus subtilis biofilms

A DISSERTATION PRESENTED
BY
NAVEEN NEIL SINHA
TO
THE SCHOOL OF ENGINEERING AND APPLIED SCIENCES

IN PARTIAL FULFILLMENT OF THE REQUIREMENTS
FOR THE DEGREE OF
DOCTOR OF PHILOSOPHY
IN THE SUBJECT OF
APPLIED PHYSICS

HARVARD UNIVERSITY
CAMBRIDGE, MASSACHUSETTS
AUGUST 2013

Thesis advisor: Michael P. Brenner and David A. Weitz Naveen Neil Sinha

Visualizing patterns of gene expression in growing Bacillus subtilis biofilms

Abstract

Most bacteria live in surface-attached colonies known as biofilms, which contain distinct cell types embedded in a self-produced extracellular network of polymers. Differentiation into functionally-distinct sub-populations of cells, or phenotypes, is primarily a result of nutrient availability and extracellular signals. These inputs change over time, leading to spatial and temporal patterns in the relative populations of phenotypes. Although transitions between phenotypes have been investigated in single cells, the triggers for this process within an intact biofilm are not well understood.

Here we demonstrate a method for measuring spatiotemporal patterns of gene expression in growing bacterial biofilms and quantitatively linking these patterns to external cues. *Bacillus subtilis* is our model system, since the pathway to sporulation includes just three phenotypes. We use a triple-labeled strain of bacteria, so that the gene expression for each phenotype is linked to a different fluorescent protein. We are able to quantify the sub-populations for each phenotype from fluorescence microscope images, once we correct for the optical properties of the biofilm. By taking into account the local growth rate throughout the colony, we are able to calculate the transition rates between different phenotypes. This technique opens up new possibilities for studying how nutrient levels and other growth conditions affect the development of bacterial biofilms.

Contents

Listing of figures

To my parents.

Author List

I am grateful to Agnese Seminara for help with the mathematical models, James Wilking for assistance with the experimental methods, and Stephan Koehler for advice with the Matlab code.

Appendix A is adapted from "Science and Cooking for Undergrads: The Kitchen as a Physics Classroom", a paper co-written with Amy Rowat and Pia Sörensen, which was submitted to the American Journal of Physics.

Appendix B is adapted from "Cocktail Physics", co-written with David Weitz, which appeared in Physics World, **24**(12), 25-28, (2011).

Acknowledgments

The serendipitous path to this thesis was possible thanks to an amazing network of people: applied mathematicians, physicists, microbiologists, designers, teachers, bartenders, and chefs, among others.

Having two advisors with insightful, yet complementary, attitudes has transormed my outlook on scientific research. Michael Brenner's enthusiasm led me to spend many nights attempting to film fruiting bodies in biofilms, bake hundreds of cookies with the help of America's Test Kitchen, and do more in three months than the previous three years. David Weitz's combibation of curiosity and criticism allowed me to perform science demos at the South Beach Food and Wine Festival, learn soft matter physics lessons at the best cocktail bar in the world, and push myself to articulate what I *really* learned from an experiment.

One benefit of working on such an interisciplinary project was being able to interact with a range of faculty. Katia Bertoldi and Vinny Manoharan provided useful feedback throughout my grad school track, starting with my early forays into the rheology of chocolate. Both Rich Losick and Roberto Kolter are last authors on many of the papers that I cite, so I was fortunate to be able to talk directly with them. Fortuitously, Shmuel Rubinstein returned to Harvard after several years abroad and gave crucial feedback towards the end of my project.

Jim Wilking showed me that "sometimes the old ways are the best" and has a fantastic intuition for doing experiments. Agnese Seminara provided a

mathematical framework for all my work and was always happy to answer questions, even from across the Atlantic. Stephan Koehler took my coding and analytic skills to the next level.

Outside my immediate circle of collaborators, I was fortunate to have the help of many wonderful post-docs. Tommy Angelini trained me in the essential skills of making media, pouring plates, and spotting colonies. Hera Vlamakis did ground-breaking work that was the inspiration for my research and taught me the basics of *Bacillus subtilis*. Rachel Dutton and Ben Wolfe were alwas helpful with my microbiology questions. The BASF Biofilm group, including Marc Schroeder and Oliver Caplan, provided a sense of continuity throughout all five years. I am especially grateful for the help of Matt Cabeen, who created the triple labeled strain that enabled the striking time-lapse movies.

The Science and Cooking course was an unexpected detour that changed my career path and introduced me to a whole new network of people. Amy Rowat and Otger Campás worked behind the scenes to make the course a reality. Daniel Rosenberg also made the course possible through his ability to put together demos at the last minute. Héloïse Vilaseca was instrumental during the second year of the course by managing the lab and coordinating with the chefs. I am grateful to Pia Sörensen for taking over many of the logistics I dealt with the first year. Christina Andujar and Kathryn Hollar gave me incredible opportunities for science outreach, including developing the curriculum for the first Harvard Science and Cooking for Kids program.

Through the Science and Cooking course, I made numerous connections throughout the culinary world, including several good friends. Jason Doo gave me a fascinating glimpse into the world of a chef and Geoff Lukas inspired me with his scientific curiosity about food. Dan Souza and America's Test Kitchen played a crucial role in Michael Brenner's project to mathematically understand baking recipes. John Gertsen, Dave Arnold, and Harold McGee deepened my appreciation for cocktails while writing a Physics World article with David Weitz.

Whether I was filming bacterial colonies or helping my advisors with the Science and Cooking course, my labmates were an exceptional source of support.

In the Weitz Lab, I am especially grateful for the help of Adrian Pegoraro, Allen Ehrlicher, Connie Chang, Don Aubrecht, Helen Wu, Joe McDermott, John Heyman, Liheng Cai, Lloyd Ung, Lolo Jawerth, Max Zieringer, Ming Guo, Sorell Massenburg, Stefan Munster, Peter Lu, Tina Lin, and Tom Kodger. Across the hall in Vinny Manoharan's lab, I was fortunate to get to know Anna Wang, Becca Perry, Sofia Magkiriadou, Nick Schade, and Tom Dimiduk. Beyond the fifth floor of McKay, I also want to thank John Kolinski, Jon Russell, Ronn Friedlander, and Sophia Botyanszki.

Outside of lab, a strong network of friends maintained my optimism through years of failed experiments. I am grateful for Elizabeth Jarrard's positive outlook on life and constant encouragement. Kevin Liu dissected all my quandaries with a military discipline and I wish I had followed more of his advice. Johnny Siever's enthusiasm for design and eye for effective prose were both sources of inspiration. Two of my best friends from college, John Rutherford and A.J. Kumar, also moved to Boston and provided a sense of camaraderie. Andrew Leifer helped me throughout my undergraduate Physics courses and shared the LaTeX template for this document. Lauren Hartle helped give me hope through the final sprint to the finish line. Improv comedy totally changed my outlook on life, and I am particularly grateful to Chris Duffy for helping me see new connections in my research. The team at Commonwealth CrossFit also changed my world view and gave me motivation to accelerate my research progress. My roommates, Patrick Herring, Brendan Shields, and Shaw Saw made my apartment a welcome place to return after the highs and lows of lab life.

Finally, I am deeply grateful for the support of my family: Dipen Sinha, Barbara Sinha, Beverly Sinha, Betty Hileman, and Cassie Beck.

1

Overview

My unconventional journey through grad school is reflected in this thesis; although there was no master plan at the outset, my major research projects reflected a similar style of solving problems. In each case, I explored a complex soft matter system with hundreds of variables, then established a quantitative framework for starting to understand its behavior.

Structure of this thesis

My focus throughout the PhD program was biofilms, but I applied a similar problem-solving mindset to the Science and Cooking class and the physics of cocktails.

Biofilms

Chapter 2: Introduction to Phenotype Expression in Biofilms

Cheese rinds, dental plaques, and the gut microbiome are just a few examples of the near ubiquitous bacterial colonies known as biofilms. These colonies contain multiple types of cells, or phenotypes, held together at a surface by a polymer network. Existing techniques are unable to quantitatively track all the sub-populations of phenotypes throughout an intact, growing colony. As explained in this chapter, this limitation prevents a better understanding of the causes for transitions between phenotypes.

Chapter 3: Quantitative Time-Lapse Fluorescence Imaging

As a first step towards understanding the differentiation into multiple phenotypes, we use a specially-constructed triple labeled strain of *Bacillus subtilis*. This chapter explains how we obtain time-lapse movies of the life cycle of biofilms. We characterize the optical properties of the colonies in order to later convert fluorescence intensities into numbers of cells.

Chapter 4: Visualization of Gene Expression

Gene expression in a biofilm shows consistent radial patterns as the colony grows larger and runs out of nutrients. Surprisingly, the order of the appearance of phenotypes does not reflect a qualitative model that depends only on the concentration of nutrients in the agar substrate, as described in this chapter.

Chapter 5: Calculation of Transition Rates between Phenotypes

To go beyond observations of sub-populations of phenotypes, we measure the transitions between them. To account for cell division within the colony, we track the expansion of the colony and account for the effects of cell division and advection. In this chapter, we show how these patterns of transitions do not

match measured or simulated nutrient profiles underneath the colony, implying that active transport of nutrients and intercellular signaling is involved.

Chapter 6: Future Applications

Although we demonstrate the technique using *Bacillus subtilis* colonies grown on agar substrates, our approach can be adapted for numerous other microbial applications, such as investigating quorum sensing and exploring interactions in multi-species biofilms.

Appendices

Appendix A: Supplemental Information

This section includes a list of strains constructed for our experiments, as well as a more detailed discussion of some of the mathematics.

Appendix B: The Kitchen as a Physics Classroom

Our approach to quantitatively representing the complex transformations that occur during the growth of a biofilm can also be applied to the culinary world. In the biofilm work, we develop a novel way of representing the growth of a biofilm through radial profiles and spatiotemporal plots. Similarly, many of the processes from cooking can be quantified in terms of time, temperature, and other physical parameters, so they can be represented on phase diagrams.

Through my role as the first Head Teaching Fellow for the Science and Cooking course, I helped develop a curriculum that explains cooking using concepts from the physical sciences. This chapter describes the curriculum from the course, including both the demos from lectures and the edible lab experiments performed by the students.

Appendix C: Cocktail Physics

The world of mixed drinks can also benefit from the quantitative approach applied to biofilms and the Science and Cooking course. The vast range of recipes can be simplified in terms of time, temperature, and dilution. Concepts from the soft matter physics, such as foam and emulsions, explain the appearance and texture of these drinks.

In a project inspired by the insights from the Science and Cooking course, I interviewed several leading experts in the field to explain how tools from science are enabling advances in the world of cocktails.

2

Introduction to Phenotype Expression in Biofilms

Bacteria at surfaces form architecturally complex communities known as biofilms [1]. Biofilms have been found in environments as extreme as hot springs, deep sea vents, and drainage run-off from acid mines [2], as well as most household surfaces, such as water pipes, toothbrush bristles, shower heads, kitchen sponges, and pacifiers[3].

The near ubiquitous nature of biofilms leads to numerous problems and applications, in a variety of industrial and medical settings. Our bodies are covered by a diverse microbial community; the populations of different species have a significant effect on digestion [4] and our teeth are coated in a rich microbial community [5]. The ability of pathogenic bacteria to differentiate into matrix producing and dormant cells makes them more resistant to antibiotics in

hospitals[6][7]. Biofilms are also used for wastewater treatment [8] and microbial fuel cells [9][10]. These colonies can cause catastophic clogging in porous materials, industrial filters, and medical stents [11].

Biofilms likely evolved as a survival strategy for bacteria in stressful environments, such as high temperatures, extreme pH, intense UV radiation, and starvation [2]. The close proximity of cells in a biofilm facilitates intercellular communication, such as quorum sensing. In response to their local environment and signals from other cells, bacteria express different types of behavior. By differentiating into multiple phenotypes, a division of labor allows the overall colony to survive under a range of environmental conditions [12]. Some examples of phenotypes include the swarmer and stalked cells in *Caulobacter cresentus*, the photosynthetic and nitrogen-fixing cells in Cyanobacteria, and the active and vegetative cells in Myxobacteria [13].

The details of how bacteria within an intact colony switch between different phenotypes within a colony are not well understood. Patterns of gene expression arise in whole colonies due to variations in the local conditions around the cells. Fluorescence microscopy is frequently used to track gene expression in colonies. However, this does not provide actual populations of cells of each phenotype, which is a crucial piece of information to understand switching between them.

Here we obtain spatiotemporal patterns of sub-populations of phenotypes in a growing biofilm, by converting fluorescence intensities from microscope images to numbers of cells. The sporulation pathway in *Bacillus subtilis* offers a simple demonstration of this technique.

2.1 *Bacillus subtilis* as a model biofilm

Bacillus subtilis is a model system to study biofilm development. When deprived of nutrients to varying degrees, cells switch between three main phenotypes: motile, matrix producing, and sporulating [14], shown in Fig. 2.1.1. Motile cells have flagella, which allows them to swim in media or along agar surfaces. Matrix producing cells transport a mixture of amyloid proteins and exopolysaccharides

outside the cell wall; this links the cells together into chains. Finally, spore forming cells asymmetrically split into a mother cell, which dies, and a spore, which is a heat- and antibiotic-resistant cell that germinates under favorable conditions.

These three phenotypes are almost mutually exclusive and include the vast majority cells in a growing biofilm; additional phenotypes, such as cannibalism and protease competence, overlap with the three main phenotypes or contribute only a small fraction to the total population [13]. Cells stochastically express several of the genes in the regulatory network, to allow more rapid switching when environmental conditions change [15]. Feedback loops ensure that most cells are expressing only one of the three phenotypes [14] [16]. The transitions between these phenotypes are controlled by SpooA, a master regulator protein. Extracellular signals can phophorylate SpooA, leading to the active form SpooAP~. At low concentrations of SpooAP~, cells are motile. At intermediate levels of SpooAP~, *Bacillus subtilis* produces the components for the extracellular matrix [17]. At the highest concentration of SpooAP~, cells form spores.

2.2 Causes of transitions between phenotypes

The phenotype of a cell primarily depends on its local environmental conditions. This is sensed either directly through receptors in the cell wall or indirectly through shifts in a cell's metabolism, based on access to nutrients. Small molecules, including nutrients, are transferred through the cell membrane by transport membrane proteins[18]. A deficit of nutrients within the cell can change the rate of specific intercellular reactions, leading to changes in the gene expression [19]. Histidine kinase proteins in the cell wall detect molecules just outside the cell, which include extracellular signals, toxins, and nutrients [20]. These transmembrane kinases activate specific genetic pathways, which determine the cell's phenotype.

Bacillus subtilis contains four main kinases: KinA, KinB, KinC, and KinD. The

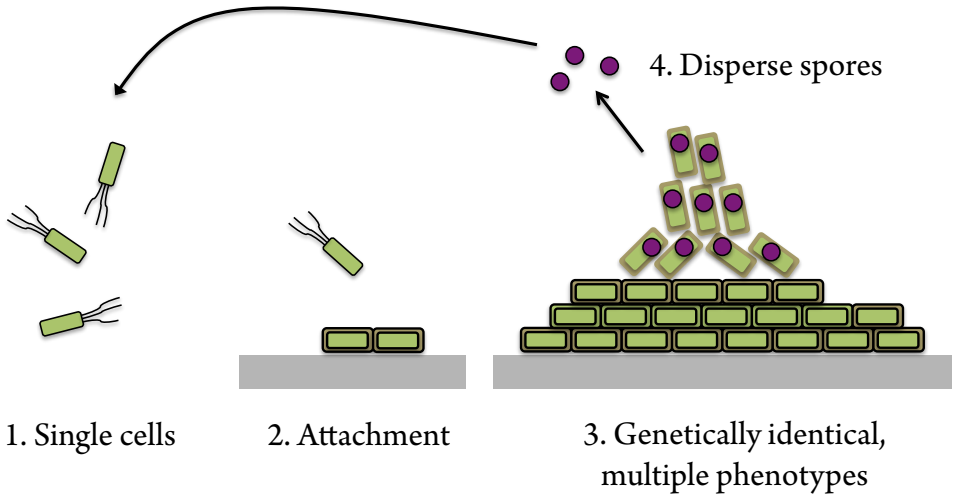

Figure 2.1.1: Typical life cycle of a biofilm. 1) Bacteria often begin as motile cells in liquid culture. 2) Cells excrete a mixture of polymers, called matrix, which binds the cells together and adheres them to a surface. 3) Even genetically identical cells differentiate into multiple phenotypes. 4) At the end of the biofilm's life cyle, cells produce spores that germinate to start new colonies. Note that this is only a representative example; not all species follow this pathway to sporulation.

exact role of each kinase is unclear. KinA may not actually respond to an extracellular signal, but instead changes caused by nutrient deprivation within the cell [19]. KinA and KinB may work together to sense access to oxygen [20]. KinC detects membrane damage and potassium ion leakage, which can be caused by the signaling molecule surfactin [12][21]. KinD probably senses osmolarity [21] [22], since it independently detects both extracellular matrix [23] and a small molecule released from the roots of tomato plants [24].

The molecules that act as cellular inputs often travel by diffusion, a slow mode of transport for distances comparable to the largest dimensions of biofilms. The time required to diffuse a distance d is given by the diffusion time $t_d \approx d^2/D$, where $D \approx 10^{-5}\text{cm}^2/\text{s}$. Even for a short distance compared to the radius of the colony, 0.1 cm, $t_d \approx 10^3\text{s}$. This limitation leads to variations in local environmental conditions, which causes spatial variation in the expression of different phenotypes [25]. Not surprisingly, the kinases show spatial regulation;

KinA and KinB are active in the older, central regions of the biofilm, and KinC and KinD are active in the younger, peripheral regions [26].

2.3 Existing techniques for studying biofilms

Fluorescence microscopy is a powerful technique for monitoring the spatial distribution of phenotypes. This is achieved experimentally by linking production of a protein to the promoter for the relevant genes. Previous work using fluorescently labeled cells shows spatial regulation in the patterns of motile, matrix-producing, and spore-forming cells [27] and kinase activation [26]. In our work, we use labels for all three phenotypes, as shown in Fig. 2.3.1. A red fluorescent protein, mKate2, is produced in motile cells, a blue fluorescent protein, cfp, is produced at the same time as the components of the matrix, and a green fluorescent protein, citrus, is produced late in the sproulation process.

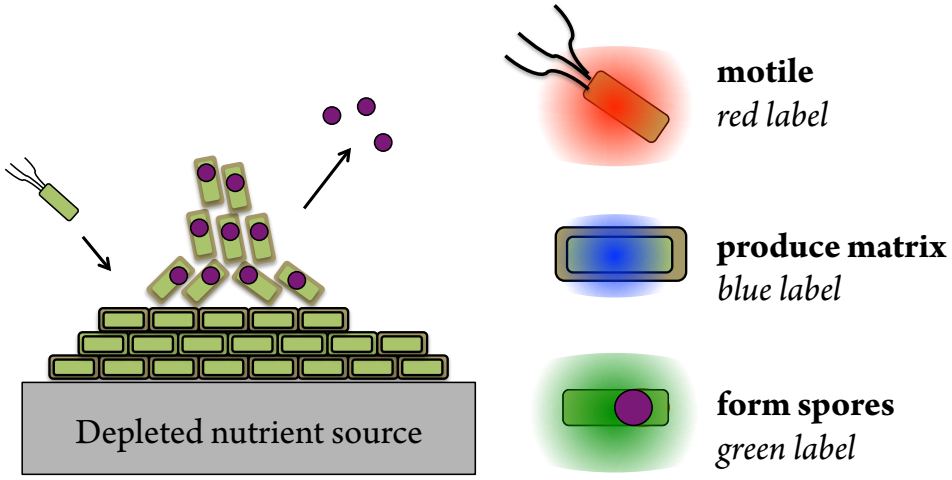

Figure 2.3.1: Labeling cells with fluorescent proteins. When motile, cells express a red fluorescent protein: mKate2. When producing matrix, cells express a blue fluorescent protein: cfp. When cells are forming spores, they express a green fluorescent protein: citrus.

To obtain quantitative information about cell sub-populations, flow cytometry of fluorescently labeled cells is the most common method [27]. With this

technique, biofilms are scraped from an agar substrate, resuspended in liquid, and the phenotypes of each cells are individually counted by a laser and photo-detectors. Unfortunately, this technique is destructive and it is difficult to extract cells from a sub-mm size area of the colony for high spatial resolution.

In this work, we develop a technique that combines the spatial and temporal capabilities of fluorescence microscopy with the ability to quantify sub-populations of each phenotype. This involves two main advances over existing methods. First, the triple labeled strain allows tracking of all the cells within a colony. Second, adjustment for the optical parameters of the biofilm allows conversion of fluorescence intensities into numbers of cells.

Table 2.3.1: Features and Limitations of Existing Techniques

Technique	Spatial Info	Temporal Info	Non-destructive	Quantify sub-pop.
Fluorescence microscopy				
Single cell		✓		
Thin sections	✓			
Whole colony	✓	✓	✓	
Flow cytometry		✓		✓
Current approach	✓	✓	✓	✓

By combining these two types of information, we quantitatively measure the fraction of cells present at each location in the colony over time. With quantitative information about cell populations, we determine the transition rates between different phenotypes, in order to explore their connection to nutrient levels and intercellular signaling. This approach is explained over the next three chapters.

3

Quantitative Time-Lapse Fluorescence Imaging

How do we track the phenotypes of all the cells in a bacterial colony during its life cycle? Here we demonstrate two advances in fluorescence microscopy that enable quantification of phenotype sub-populations throughout a biofilm. First, we construct a triple labeled strain that allows us to monitor the three predominant phenotypes throughout a *Bacillus subtilis* biofilm. Second, we characterize the optical properties of the colony to convert fluorescence intensities to cell populations.

3.1 Triple labeling of cells

Accurate tracking of all the phenotypes is simplest if each phenotype has a unique fluorescent label. We use phage transduction to create a triple labeled strain. Each cell contains three pairs of linked proteins and promoters; when the relevant promoter for a phenotype is expressed, a fluorescent protein is also produced.

3.1.1 Strain construction

We track the expression of each phenotype by fusing a gene encoding a fluorescent protein to the promoter for the relevant gene. Phage transduction allows insertion of the genes into the bacterial DNA. We follow general methods for molecular cloning to construct strains according to established protocols [28]. Introduction of DNA into our lab strains is conducted via transformation [29]. SSP1 phage-mediated general transduction is used to introduce antibiotic resistance marker-linked mutations or reporter fusions into derivatives of the 3610 strain of *Bacillus subtilis* [30]; the antibiotic resistance selects for only cells that have the reporter fluorescent protein fused to the desired promoter.

For the majority of our studies, we use a strain with three different fluorescent labels, each at a different locus along the biofilm genome. Below are more details about the specific promoters used to track each phenotype.

1. **Motility** is linked to the *hag* promoter, which is responsible for flagellin production [31].

2. **Matrix production** is linked to the *tapA* promoter, which is part of the *tapA-sipW-tasA* complex. The *tapA* gene produces the amyloid proteins, *tasA* produces the polysaccharide, and *sipW* enables transport of both of these components outside the cell [32].

3. **Sporulation** is linked to the *sspB* promoter, which encodes a small, acid-soluble protein that is found in late-stage spore formation [27]. After

forming spores, cells do not fluoresce, so the fluorescence intensity is an under-representation of the total number of cells that have sporulated.

All strains used in this study are listed in the Supplemental Information.

3.1.2 Colony initiation and incubation

We grow colonies on 1.5 wt% agar gel with a minimal media, MSgg, designed to induce biofilm formation and sporulation: 5 mM potassium phosphate (pH 7) 100 mM MOPS (pH 7) / 2 mM $MgCl_2$ / 700 µM $CaCl_2$ / 50 µM $MnCl_2$ / 50 µM $FeCl_3$ / 1 µM $ZnCl_2$ / 2 µM thiamine / 0.5% glycerol / 0.5 % glutamate / 50 g/ml tryptophan / 50 g/ml phenylalanine. The agar solution is cooled to 55°C before adding the remaining ingredients. We typically use 100-mm diameter petri dishes containing 15 mL of media, to delay nutrient deprivation at the perimeter of the colonies. The plates are covered with lids and cooled overnight at room temperature, then spotted within 24 h, since refrigeration changes the morphologies of the resulting colonies.

Strain NCIB 3610 is used for all experiments [33]. While the plates are cooling, strains are grown from freezer stock in approximately 3 mL of shaken Luria-Bertani (LB) at 37° C. Before inoculating the plates, we remove the lids and allow the surface to dry for 5 – 10 minutes. We used two different methods to transfer the bacteria to the surface of the agar. For larger colonies, we spot with 0.5 μl of bacterial culture at $OD_{600} = 1$. For smaller colonies, we use a sharp wooden stick dipped in the bacterial culture to gently poke the surface of the agar. In both cases, we allow the drop to dry for 5 – 10 additional minutes with the lid off until the meniscus of the initial drop is no longer visible and the bacteria are left in a "coffee ring" around the perimeter.

For time-lapse movies, we grow colonies in a Tupperware container stuffed with wet paper towels and sealed around the microscope objective using Glad Press'n'Seal plastic wrap. The temperature of the microscope is maintained at 32° using heating elements and fans.

3.1.3 Optimization of the growth protocol

We vary the dimensions of the agar gel and the colony inoculation protocol to optimize the growth of the colonies. To minimize the time needed to run each experiment, we aim for small colonies that rapidly sporulate. We also seek to minimize the thickness of the colony, to reduce the effect of attenuation, without qualitatively changing the morphology of the biofilms. 100 mm diameter plates with a 2 mm thick agar gel are optimal. By poking the surface with a wooden stick dipped in bacterial solution, rather than using a micropipette, we obtain a larger dynamic range of colony size than with the micropipette. Alternatively, we use a pulled glass tube with a small ($\approx 50\mu$m) opening to consistently place small liquid drops on the surface.

3.2 Optical setup

We use a Zeiss Lumar Stereoscope for imaging whole colonies. A Schott KL 2500 LCD halogen lamp provides illumination for brightfield imaging. The 0.8x objective on the stereoscope allows up to a 2.3 cm field of view, which is larger than the final size of the biofilms. For simultaneously monitoring the three fluorescence channels, we use three different filter sets. Each set contains one bandpass filter to select the wavelengths used to excite a particular fluorophore and one bandpass filter to select the wavelengths emitted by that fluorophore: 1) the CFP filter set (Zeiss # 486047) Excitation Bandpass (BP) Filter 436/20 and Emission BP 480/40, 2) the RFP filter set, and 3) the YFP filter set (Zeiss # 486046) Excitation BP 500/25; Emission BP 535/30. All images are recorded with a Zeiss Axiocam MrM. The spatial resolution of the images is 12 μm/pixel for most our experiments.

To account for fluctuations in the transmitted light, we normalize the transmitted light intensities by the average intensity in one corner of the image. To minimize spatial variations in the white light illumination, we use a thick plastic diffuser from a gel electrophoresis setup.

Data are saved as 16-bit gray-scale TIFF files, since the camera has 12-bit resolution. We do not auto-scale the data before saving.

3.2.1 Verification of cell-labeling

To verify that fluorescence in each channel is only from the corresponding fluorescent protein, we observed fluorescence from single-labeled strains using all three filter sets, as shown in Fig 3.2.1. There is almost no overlap in the excitation wavelengths of the fluorophores, although we observe slight autofluorescence with the CFP filter set. The autofluorescence is likely the result of the pigment, but only occurs after 48 h; most of our movies last only 36 hours so this is not an issue.

3.3 Calibration for biofilm optical properties

To convert the fluorescence intensities into numbers of cells, we need an independent way to measure the total number of cells. Ideally, we could add a constitutive reporter to the cells, so that the intensity of that signal would be directly related to the number of cells. Unfortunately, this is not feasible due to potential overlap in the wavelengths of the other three fluorophores, so we use transmitted light to indirectly measure the total population. For calibration between fluorescence and cell population, we use a separate constitutively labeled colony. To apply the results from the constitutively labeled colony to the triple labeled ones, we compress a segment of the colony to a known spacing between two glass coverslips, as described in the next section.

3.3.1 Transmitted light attenuation

We assume that the number of cells is proportional to the total volume of the colony, and use the height of the colony as an indicator of the total population. Most high-resolution techniques for measuring height profiles, such as

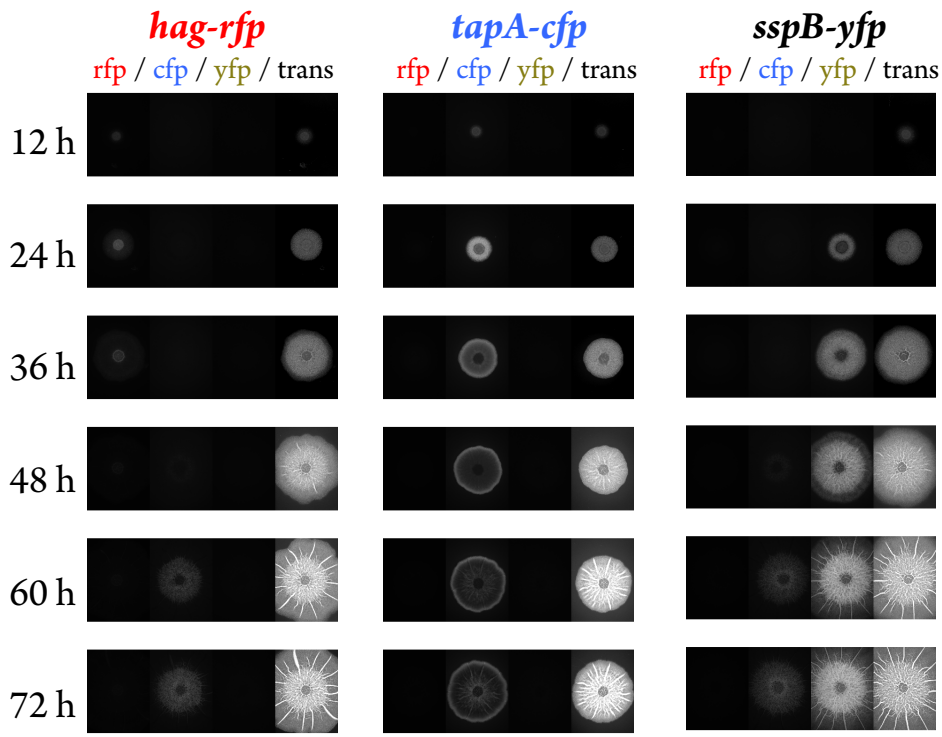

Figure 3.2.1: Single labeled biofilms. We take images of single labled biofilms over time to check for any cross-talk in fluorescence. Each column corresponds the age of the colony. From left to right: only motility, matrix production, or spore formation are labeled. Autofluorescence in the cfp channel occurs with all strains.

profilometry or confocal microscopy, cannot be performed simultaneously with the wide-field fluorescence microscopy. Stereo imaging potentially solves this problem, but further work is needed to demonstrate the sensitivity of this technique. However, the attenuation of transmitted light by the biofilm material provides a simple way to measure the height at every position in the colony.

By calibrating the light attenuation through the colony, we are able to estimate the thickness of the colony. We compress biofilms between glass coverslips separated by calibrated spacers, in order to measure the dependence of biofilm material thickness on light transmission. These spacers are made from polystyrene and range in thickness from 10 μm to 750 μm (Atrus, color-coded

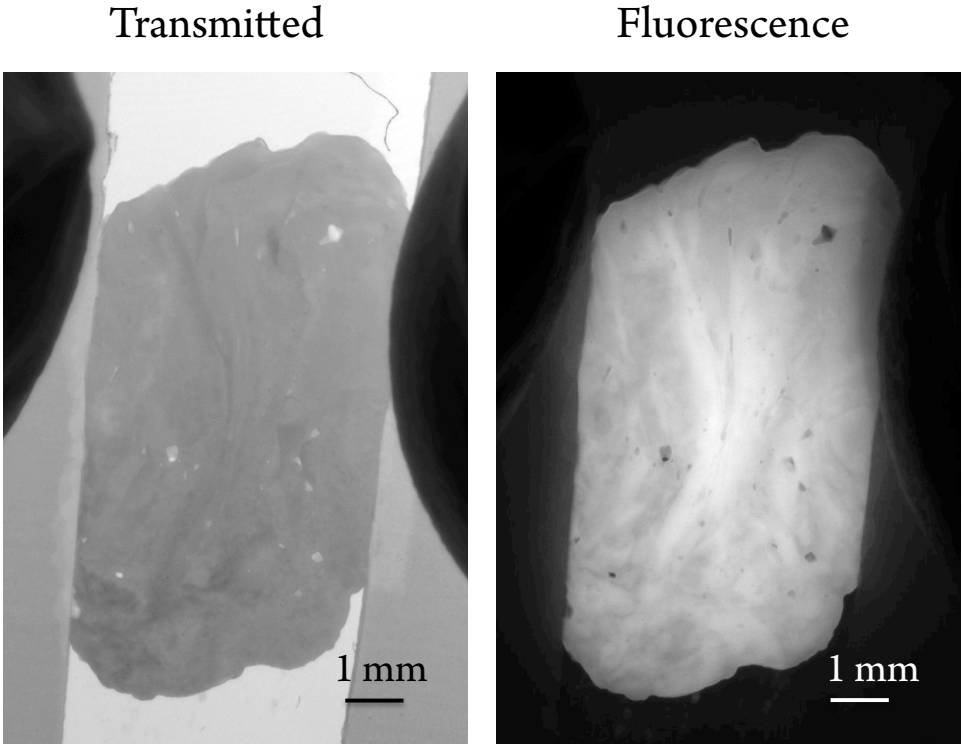

Figure 3.3.1: Constitutively labeled biofilm segment. The left image shows the intensity of transmitted light through a section of biofilm, from a strain constitutively labeled with the mKate2 red fluorescent protein. The right image shows the same section of biofilm, as observed with the RFP settings of the microscope. In both images, the biofilm is compressed between glass coverslips separated by 250 μm. The scale bars correspond to 1 mm.

optical shims). The coverslips are compressed together and no water is expelled from the biofilm material, so we assume that the density of the material does not change.

In the ideal case, the biofilm material would be homogeneous, but we observe that the fluorescence and transmitted light intensity are non-uniform across the area of the compressed biofilm, as shown in Fig. 3.3.1. For each biofilm image, we measure the mean and standard deviation of the distribution in fluorescence intensity throughout the area of the biofilm. Attempts to homogenize the bacteria result in air bubbles, which prevent accurate calculation of the height.

The attenuation of white light approximately follows an exponential decay with thickness; this allows us to calculate the height of the colony over time, $h(t)$, from the intensity at each point $I(t)$, the background intensity $I_0(t)$, and an attenuation coefficient $\lambda(t)$.

$$h(t) = -\lambda(t) \log \frac{I(t)}{I_0(t)}. \tag{3.1}$$

The time dependence of λ comes from a pigment produced by the colony, as described in Sec. 3.3.5.

We verify our height calculations by looking at cross-sections through the colony with a confocal microscope.

3.3.2 Fluorescence intensity calibration

This attenuation of light also reduces the intensity of the fluorescence signals, since they overlap the wavelengths of the bright-field illumination. We assume that the illumination is strong enough that all fluorophores are excited, so the attenuation only affects the emitted light. Constitutively labeled colonies allow us to determine the intensity of the fluorescence signal F as a function of colony thickness. In the absence of attenuation, the signal would increase linearly with the number of cells; with attenuation, if the fluorophores are uniformly distributed along the z-axis, the signal decays as $\left(1 - e^{h(r,t)/\lambda(t)}\right)$, where λ could be different for each wavelength.

3.3.3 Mathematical model of attenuation

These trends in transmitted I and fluorescence F_i light intensities are explained with a simple mathematical model, where i denotes the phenotype of the cells. To simplify the notation, we will now write λ for $\lambda(t)$. The multiple scattering is negligible, so the transmitted light intensity at each z position is described by:

$$\frac{dI(z)}{dz} = -\frac{I(z)}{\lambda} \rightarrow I(z) = I_0 e^{-z/\lambda}. \tag{3.2}$$

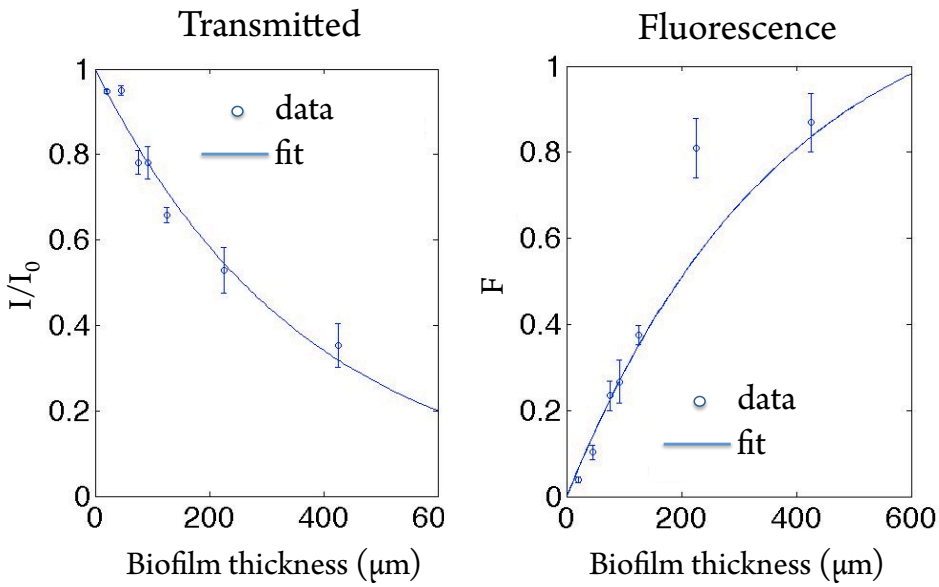

Figure 3.3.2: Attenuation due to biofilm material. *Left*. Ratio of transmitted I to incident I_o light as a function of biofilm thickness. The intensity decays exponentially with a length-scale $\lambda = 372\mu$m. *Right* The same attenuation length-scale applies to the fluorescent signal, with the addition of a linear increase in intensity with the number of cells. The fluorescence per unit height of the linear increase is 9.9 μm^{-1}.

The constant I_o corresponds to the light transmission outside the colony, when $z = 0$. By integrating across z and solving for the height h, we obtain Eqn. 3.1.

We determine the attenuation coefficient λ from an exponential fit of the measurements of light transmission (I/I_o) through a biofilm as a function of thickness. Simultaneously, we measure the fluorescence intensity F from the constitutively labeled biofilm segment. The results for a 48 hour colony are shown in Fig. 3.3.2. For the fits, the same value of λ is used for both plots, but a more accurate approach is to calibrate λ for each fluorophore.

For the fluorescent light signal, we label each phenotype with an index, so that $i = 1$ is motility, $i = 2$ is matrix production, and $i = 3$ is sporulation. We assume that each cell produces fluorescent light with intensity F_i^{on} when the promoter is expressed and a background level F_i^{off} when the promoter is not active. Outside the biofilm, the intensity of the fluorescence signal is F_{io}. For a total number of

active cells n_i, the total fluorescence intensity $F_i = n_i I^{on} + (n - n_i) I^{off}$. For a significantly low background intensity $I^{off} \ll I^{on}$, this simplifies to $F_i \approx n_i I^{on}$. Because vertical stratification occurs in biofilms, we approximate the intensity at each depth within the colony by the average fluorescence emitted per unit height $n_i F_i^{on}/h$, where h is the total height of the colony.

$$\frac{dF_i}{dz} = \frac{n_i F_i^{on}}{h} - \frac{F_i}{\lambda} \rightarrow F_i(z) = F_{io} e^{-z/\lambda} + n_i F_i^{on} \frac{\lambda}{h} \left(1 - e^{-z/\lambda}\right). \tag{3.3}$$

Substituting $z = h$ and solving for n_i we obtain:

$$n_i = \frac{h}{\lambda} \frac{F_i(h) - F_{io}}{F_i^{on}} \frac{1}{1 - e^{-h/\lambda}} + \frac{h}{\lambda} \frac{F_{io}}{F_i^{on}}. \tag{3.4}$$

A more refined version would use $\lambda_i(t)$, adjusted for how the attenuation changes for each fluorophore wavelength over time.

3.3.4 Verification of oxygen availability

The rate-limiting step in the production of fluorescent proteins requires oxygen, which can be depleted in a dense microbial community. This has been observed in yeast and bacterial biofilms. To determine if oxygen depletion is relevant for our *Bacillus subtilis* biofilm colonies, we image cross-sections of constitutively labeled *Bacillus subtilis* colonies at three relevant time points: 24h, 48h and 72h.

For each measurement, we encase the biofilm in agar to maintain its shape while cutting cross section; we cover the colony with an aqueous autoclaved agar solution (1.5 wt %) that is cooled to 40 °C. The agar is solidified for 10 minutes at 10 °C before cutting a cross-section of the agar-biofilm-agar slab for imaging. The cross-sections are imaged using fluorescence confocal microscopy, for greater spatiral resolution. Dark regions are observed in the center of the 48 h colony and the top of the 72 h colony as a result of the dark, sporulated cells. However, we do not observe a decrease in fluorescence with increasing depth into the biofilm. Therefore, oxygen depletion does not significantly affect the fluorescent protein

in the biofilm. Representative microscopy images for the three time points are shown in Fig. 3.3.3.

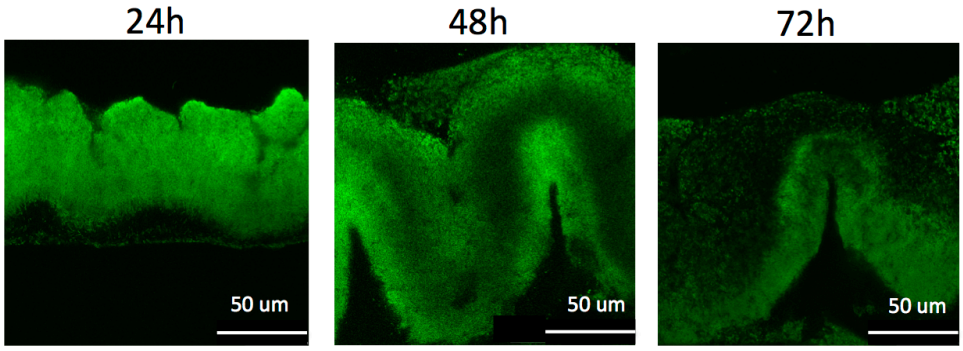

Figure 3.3.3: Cross-sections of a constitutively labeled biofilm. We encase a biofilm in agar, then slice along a diameter to determine the penetration depth of oxygen into the colony. We repeated the experiment for three different time points: 24h, 48h, and 72h. The dark regions probably correspond to cells that have sporulated, since they do not fluoresce. However, we do not observe a decrease in fluorescence with increasing depth into the biofilm. Therefore, oxygen depletion does not significantly affect the fluorescent protein in the biofilm.

3.3.5 Potential sources for fluorescence variability

Although these models fit well for our particular biofilm system, we make several simplifications that may not be valid for other labeled strains or colonies. Below are additional details about the potential complications mentioned above.

Fluorophore production

The gene fluorescent protein is fused to a promoter; the particular promoter used to track each phenotype could be expressed at a different rate. Flow cytometry data shows that motile cells exhibit a fairly uniform distribution of fluorescence intensity per cell, matrix-producing cells exhibit a range of intensities, and spore-forming cells exhibit a bimodal distribution of intensity [27].

Several factors may affect the timing of the expression of fluorophores. The activation of the promoter may be delayed from upstream changes leading to the

phenotype transition. Moreover, the fluorophore has a finite lifetime before it is digested by proteins within the cell. We assume that the fluorescence per cell is constant throughout the course of the experiment for the motile and matrix-producing cells. The promoter used to track sporulation, *PsspB*, is expressed late in sporulation, but not in mature spores [27], so we assume that the fluorescence disappears after the spores are mature.

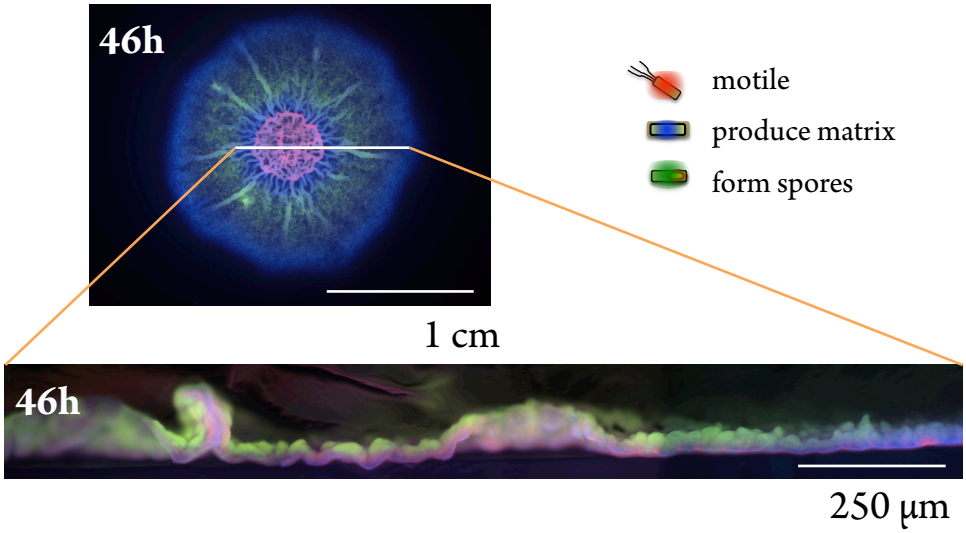

Figure 3.3.4: Vertical stratification of phenotypes. In a slice taken through a 46 hour old colony, spore-forming cells (green) are preferentially found near the top of the colony, whereas motile (red) and matrix-producing (blue) cells are found towards the bottom of the colony.

Vertical stratification

Due to attenuation of light passing through the biofilm, the intensity of the fluorescence signal of a cell depends on its depth within the colony. This dependence on vertical position makes it difficult to reach a unique solution for the sub-populations of phenotypes at each radial location; the same signal could correspond to a few cells near the surface or many cells closer to the agar. The different phenotypes do segregate into different layers of the biofilm at later

times, as shown in Fig. 3.3.4. To create the image, a 46 hour biofilm was sliced along a diameter with a metal blade and the cut surface was imaged using a higher magnification with the microscope. However, since the attenuation length is longer than the thickness of the colony, our results are still valid.

Along a vertical column, the volume fraction of cells may not be constant. The non-fluorescent space could be filled with matrix or dead cells, but other studies have shown that the total number of dead cells in a colony is not a substantial fraction of the total [34]. Changes in the volume fraction of extracellular matrix may shift our results slightly.

Pigment production

The biofilm produces a pigment in the later stages of biofilm development, which changes the attenuation of the colony material over time. The function of this pigment is poorly understood [21], but it appears to be a non-enzymatically produced water-soluble molecules that depend on the intercellular pH [35]. This pigment primarily absorbs in the UV – visible range, so to minimize the effect of the pigment on our optical measurements, we instert a long pass filter into the transmitted light path. We compare images with and without an IR filter (850 nm long pass filter) in the transmitted light path in Fig. 3.3.5.

Our calibration steps demonstrate that we collect signals throughout the entire thickness of the fluorescently labeled biofilms. By characterizing the optical properties of the biofilm, we correct for the attenuation of the biofilm material, so that we can represent the data in terms of numbers of cells. The next chapter shows how further analysis of the time-lapse images allows calculation of the fraction of each of these phenotypes relative to the total population.

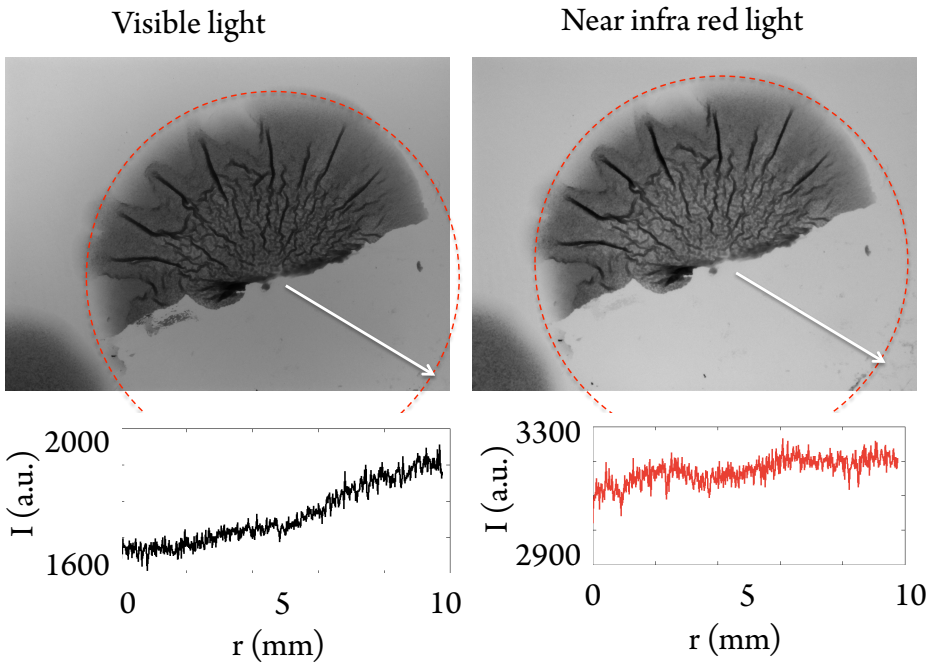

Figure 3.3.5: Correction for pigment using IR filter. Both images show a biofilm grown on an agar plate; half the colony has been scraped away to reveal the agar beneath it. *Left*. With the regular band pass filter used for transmitted light images, the light intensity decays towards the center of the colony due to pigment produced by the colony. *Right* With an IR filter the transmitted light path, the transmitted light profile is more uniform.

4

Visualization of Gene Expression

How do we extract patterns of gene expression from the time-lapse movies of biofilms? We start by focusing on the radial dimension of the colony, since all the colonies grow outwards from an initial spot. A qualitative model connecting phenotype to depletion of nutrients in the agar would predict an ordering from sporulating cells in the center, through matrix-producing cells in the mid-colony, to motile cells at the edge. Surprisingly, motility is prevalent in the center of the colony and matrix production at the periphery.

4.1 Quantification of sub-populations

The time-lapse movies of the growth of the biofilms have seven dimensions of information – radial, azimuthal, thickness, time, and three fluorescence channels – making it difficult to represent the information in a compact, visual way. We use

custom Matlab software to analyze the images of the biofilm colonies. The data are stored in three-dimensional matrices of x-position, y-position, and time, then manipulated to extract quantitative information about the growth of the biofilm. Spatiotemporal plots are a useful way to represent the growth of the bacterial colonies.

Azimuthal averaging

To simplify the analysis, we take advantage of the azimuthal symmetry of the colonies. Typical colonies have a deviation from circularity by 10 %. We determine the circularity by converting the images to a binary array, finding the centroid, and creating a histogram of the distances to the boundary of the colony.

Sometime the colonies do not fall below this threshold for circularity or are not azimuthally symmetric. Radial ridges in the colony can lead to different profiles along different radial slices. To avoid errors caused by azimuthal asymmetries in the colony radius, we select relatively uniform angular sectors of the colony to analyze, as shown in Fig. 4.1.1.

During observation of a biofilm, we obtain images of the transmitted and fluorescent light intensities, $I(x, y, h)$ and $F_i(x, y, h)$, where the subscript i signifies the corresponding phenotype for the fluorescence channel. The azimuthal averaging process reduces the dimensionality to obtain $I(r, h)$ and $F_i(r, h)$. To define the radial coordinate r, we find the center of the colony and establish a cylindrical coordinate system. This requires a few intermediate steps, which are detailed below:

1. Remove the effect of constant spatial variation in the background illumination by taking the time derivative of the transmitted light image $\partial I(x, y, h, t)/\partial t$.

2. Select the subset of pixels with a time derivative larger than some threshold, to isolate the edge of the colony.

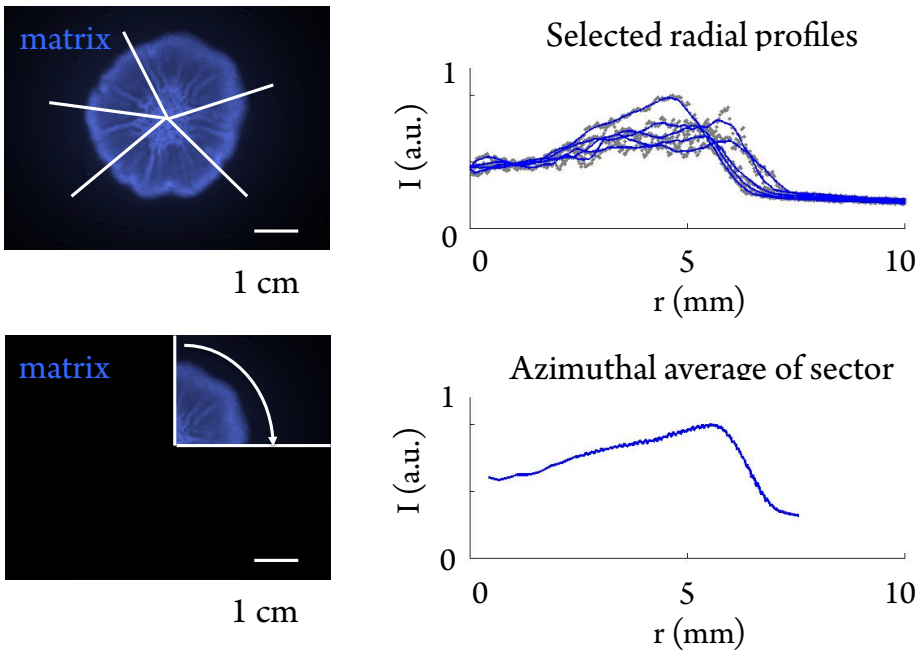

Figure 4.1.1: Azimuthal averages of biofilm images. *Top*. Some of the colonies may differ significantly from having a uniform radius and from a uniform height profile, as shown by the selected radial slices. *Bottom* By taking an azimuthal average of a small sector, we are able to minimize this variation. However, the radial patterns that we observe are robust, and do not depend on the specifics of the averaging procedure.

3. Calculate the centroid of the image from these pixels.
4. Create a grid of X and Y positions, using the `meshgrid` function in Matlab.
5. Establish a polar coordinate system relative to the centroid, using the `cart2pol` function.

A convenient way to find the radial dependence for the transmitted and fluorescence profiles is to sort the points according to the radial position. The indices of the sorted pixels are stored in a vector `r_ind`. We use the `filtfilt` function to smooth the profiles. For selecting points within an angular slice of the colony image, we use the vector `si`. For selecting points from the sorted pixels, we use the vector `ss`.

The relevant Matlab code snippet is shown below:

```
[r_sort, r_ind] = sort(rho(:), 'ascend');
r = filtfilt(ones(1,100)/100, 1, r_sort );
th = theta(r_ind);

si = ((theta>theta_min) & (theta<=theta_max));
ss = ((th>theta_min) & (th<=theta_max));
```

From these radial transmitted light profiles, we find the leading edge of the colony. Several algorithms for finding the edge are possible, including finding the point of maximum slope, finding the minimum radial position that exceeds some threshold, or interpolating the intersection with the background light transmission.

We found the third method to be the most robust, since it avoids problems caused by spatial variations in the background intensity. First we find the points on the leading edge that correspond to 40% and 70% the difference between the background and minimum light transmission values. Next we xtrapolate these two points along the radial profile to find the intersection with the background level.

To find the fluorescence profiles between the center and the edge of the colony, we interpolate the ordered vector of fluorescence intensity values. The images contain thousands of pixels, so we rescale them to a radial axis with 100 points. Specifically, for a set of radial positions `r` and a fluorescence image `red_tmp`, we use the `interp1` function to find the values along a separate radial axis, `r_azi`. At each time `j`, we set all points outside the colony `r > R(j)` equal to zero.

The Matlab snippet below shows how we calculate the radial profile for the red fluorescent protein channel, `red_azi`. The first index corresponds to radial position and the second corresponds to the time point *j*:

```
red_azi(:,j) = interp1(r, red_tmp, r_azi).*(r_azi<R(j));
```

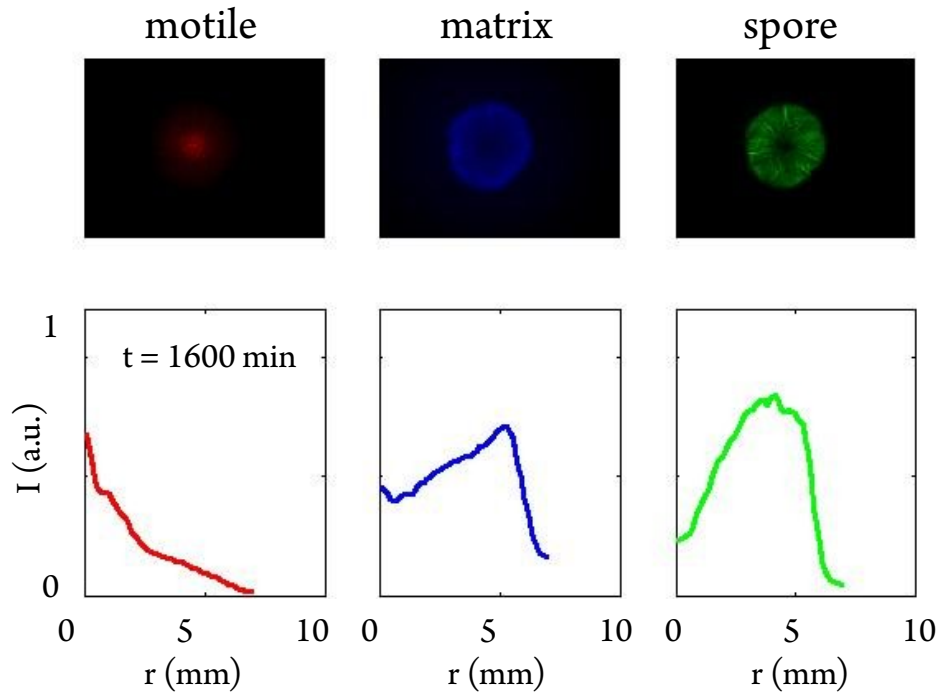

Figure 4.1.2: Radial profiles of fluorescence intensity. *Top* Images of each fluorescent channel extracted from the time-lapse movie of a 1600 min old biofilm. *Bottom* The corresponding radial profiles for each of the frames. The fluorescence intensities are in arbitrary units, normalized to one by the maximum intensity of the entire time-lapse.

This chapter focuses on the overall radial patterns, but a logical extension of this work is to repeat the analysis for a pixel-by-pixel analysis of the fluorescence microscope images.

Adjusting for differences between fluorescence channels

We calibrate the images to link fluorescence intensities to numbers of cells. Assuming all the cells fluoresce, a weighted sum of the intensities of the fluorescence profiles is proportional to the total number of cells, N_{cell}. The different coefficients for each fluorescence intensity are likely the result of differences in the efficiency of the fluorophore and the number of fluorophores per cell. We denote these coefficients by C_{red}, C_{green}, and C_{green}.

Spores do not fluoresce, but we can infer the number of spores as $N_{spore} \approx \int_0^t I_{\text{green}}(r, t') \frac{dt'}{\tau_{\text{spore}}}$, where $\tau_{\text{spore}} \approx 20\text{min}$ is the time required for sporulation. In making this approximation, we assume that the expansion of the colony is slow compared to the rate of expansion.

The sum of all these terms then becomes:

$$\begin{aligned} N\text{cell}(r,t) = C_{\text{red}} I_{\text{red}}(r,t) + C_{\text{green}} I_{\text{blue}}(r,t) \\ + C_{\text{green}} I_{\text{green}}(r,t) + C_{\text{spore}} I_{\text{spore}}(r,t). \end{aligned} \tag{4.1}$$

Assuming a constant volume fraction of cells within the colony, the thickness of the colony $h(r,t)$ is proportional to the number of cells by a constant C_0:

$$h(r,t) = C_0 N_{\text{cell}}(r,t). \tag{4.2}$$

We find the coefficients by minimizing the difference between the weighted sum of the fluorescence intensities and the scaled height profile of the colony. We use Matlab to compute this coefficients. For a height profile `h_azi`, and fluorescence profiles `red_azi`, `blue_azi`, and `green_azi`, we use matrix division to find the optimal set of coefficients to minimize the difference `err(i)` between the weighted sum and the height profiles.

```
for i = 1:size( h_azi, 2 )
    m = [red_azi(:,i), blue_azi(:,i), green_azi(:, i )];
    coeff(:,i) = m\h_azi(sub,i);
    err(i) = mean( ( m*coeff_1(:,i)./h_azi(sub,i) - 1 ).^2 );
end
```

Although these coefficients vary over the course of the biofilm's life cycle, we use the mean value for our analysis.

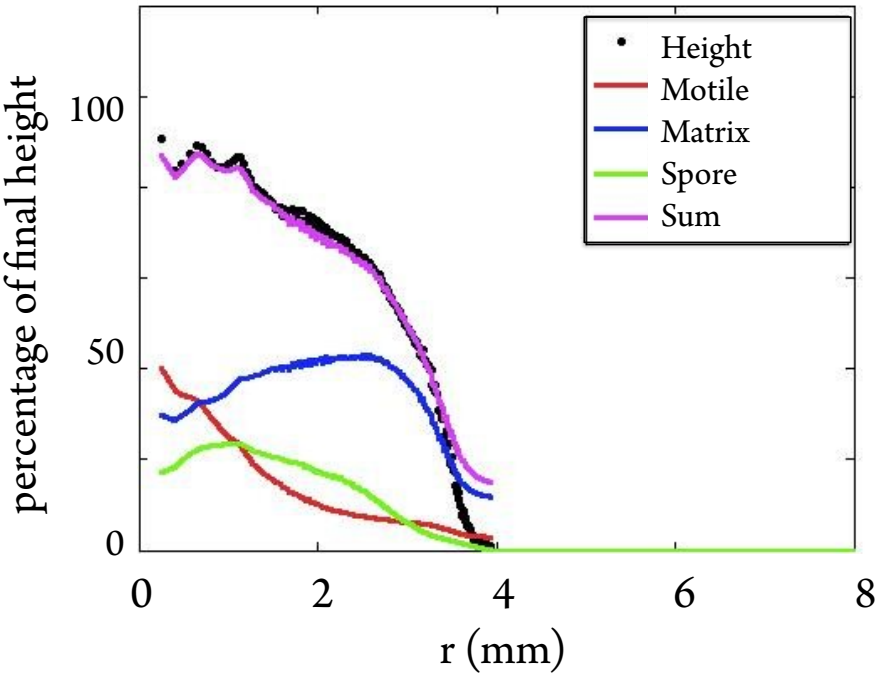

Figure 4.1.3: Weighted sum of radial profiles of fluorescence intensity. Each of the radial profiles (red, blue, and green) are multiplied by a coefficient and added together to obtain the magenta line. The profile for sporulation (green) is actually the cumulative sum of sporulating cells, because the cells stop fluorescing after the spores mature. The black dots correspond to the height profile of the colony. We find the coefficients by minimizing the difference between the weighted sum and the colony height over the entire radial profile. These coefficients vary over the life of the biofilm, but using the mean value gives a reasonable fit.

Representing radial profiles as population fractions

With these coefficients, we now represent the radial profiles as fractions of the total cell population, rather than arbitrary fluorescence intensities. Figure 4.1.4 shows the result of this transformation at one point in time, 1580 min after the inoculation. At this point, nearly half the cells in the center are motile, the edge of the colony is almost entirely matrix producing cells, and the center is a more even distribution between the phenotypes.

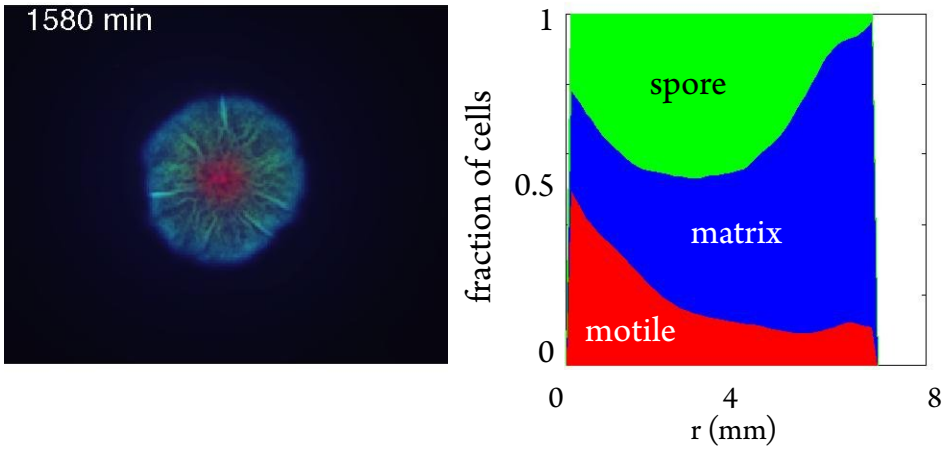

Figure 4.1.4: Radial profiles as population fractions. With the coefficients calculated from the previous section, we re-plot the radial profiles as fractions of the total cell population, rather than arbitrary fluorescence intensities. In this particular frame, motile cells are predominant cell type in the center, sporulation occupies the region further out, and matrix production occurs primarily at the perimeter of the colony.

4.2 Overview of gene expression patterns

We verify that colonies consistently exhibit the same spatiotemporal patterns of gene expression. Biofilms grow radially outwards from a small, central source of bacteria on top of an agar gel containing nutrients. This outward expansion happens in parallel with a wave of matrix production, followed by sporulation.

The relatively smooth surface buckles in later stages of the growth of the biofilm, forming wrinkles that break the azimuthal symmetry of the system. The exact pattern of wrinkles is quite sensitive to the growth conditions, such as the humidity and storage history of the agar plates. However, we generally observe wrinkles extending radially outwards from the central area of inoculation. These wrinkles are up to twice the average height of the colony. For colonies grown from a drop of liquid culture, the interior regions forms a complex network of wrinkles that protrude form the surface.

We focus on the radial patterns of gene expression in the colony, since these

show the most universal features between colonies. The sequence and radial distribution of gene expression occur consistently across colonies. The population of motility-expressing cells increases in the center of the colony during the early growth phase, then decays at later times. Matrix-producing cells are ubiquitous during young biofilms, then travel in a wave to perimeter of the colony at later times. Sporulation occurs later in the colony's life, in the region between the center and the edge. These changes are summarized in Fig. 4.2.1.

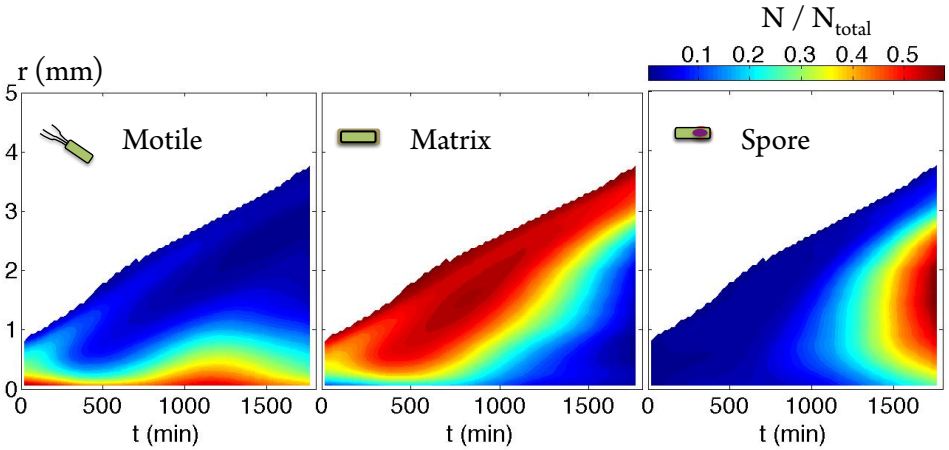

Figure 4.2.1: Spatiotemporal plot of biofilm growth. Each of the plots show the radial position relative to the center of the colony along the y-axis and the age of the colony on the x-axis. The edge of the colored region indicates the edge of the colony as it growth outwards. The color represents the fractions of each of the phenotypes: blue corresponds to zero cells and red corresponds to 50% of the population. The fraction of motile cells rises and falls over time in the center of the colony. The perimeter of the colony is mostly matrix producing cells. Near the end of the time-lapse, a majority of the cells have sporulated. The sum of the fractions is set equal to one at every point in the plot.

4.2.1 Differences from a qualitative model of nutrient flow

To interpret the results, it is useful to compare to a qualitative model of switching between phenotypes. Based on a model in which cell transitions are dependent on nutrient levels, motility would occur at the edge of the colony, sporulation at

the center, and matrix-production in between. This is different than what we observe: the edge of the colony is dominated by matrix producing cells and the center is dominated by motile cells.

Matrix production at the edge may present a selective advantage if extracellular polymer is responsible for the expansion of the colony. Previous work[36] has shown that matrix production drives growth in young colonies. The extra matrix increases the osmotic pressure within the colony, leading to a flow from the agar gel into the colony. This causes the biofilm to expand and swell outwards. To corroborate this observation, in separate experiments with higher magnification confocal fluorescence microscopy, we see chains of cells at the edge of the colony.

The rise in motility in the center is another surprising feature, since this should be the region of the colony with the lowest concentration of nutrients. We confirm this with measurements and simulations, detailed in Chapter 5. Moreover the rise in motility occurs after the rise in matrix production in the center, contrary to the expected order of differentiation.

Both of these observations could be explained if the nutrient levels experienced in the center are in fact much higher than in the agar substrate directly below the colony. Active transport through channels could transfer nutrients from the edge of the colony to the center. A magnified view of these channels is shown in Fig. 4.2.2. Previous work [37] has demonstrated fluid flow through channels underneath the wrinkles in the biofilm, making this theory seem plausible. Moreover, when placed in a nutrient rich environment, such as LB, cells can switch from producing matrix to being motile [Hera Vlamakis, unpublished]. These channels would only become established after higher levels of matrix production.

To move a step closer to mapping actual phenotypic switching, it is useful to look at plots of the time derivative of sub-populations, as shown in Fig. 4.2.3. The increase in matrix production at the center clearly precedes the increase in motility. The area of the decrease in the proportion of matrix production matches the area of the increase in the proportion of sporulating cells; this suggests

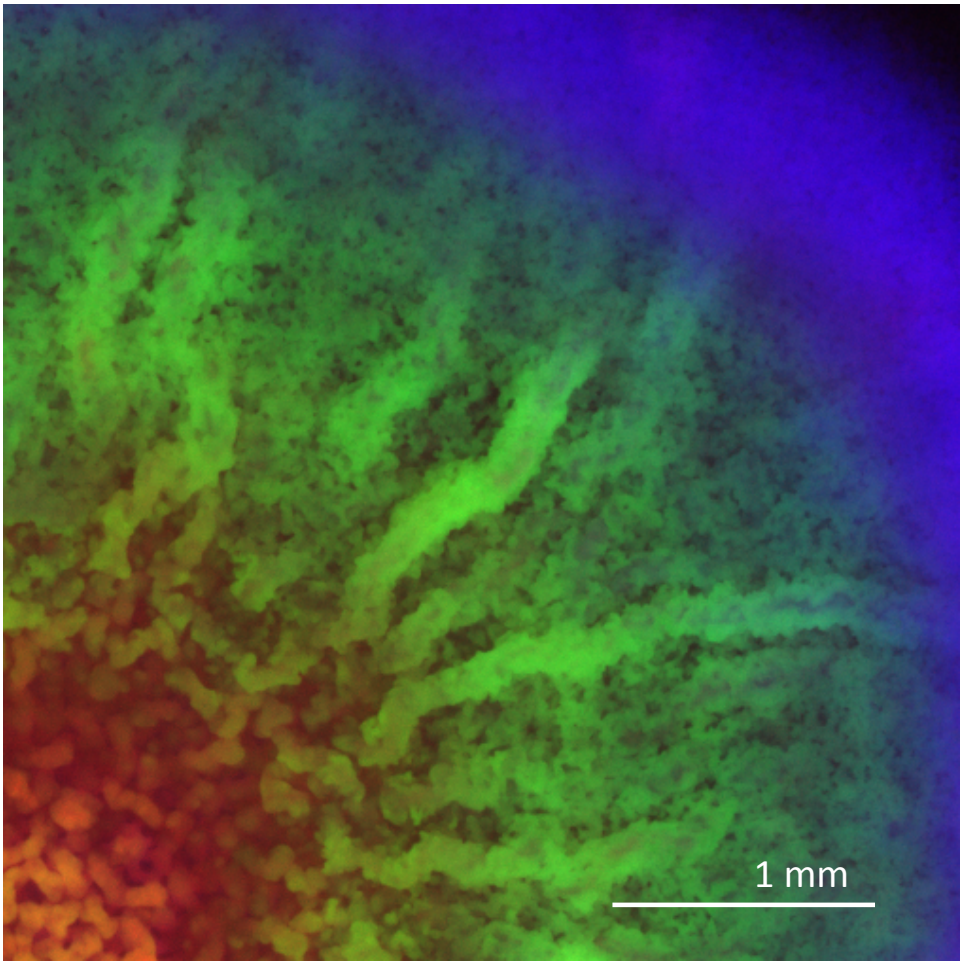

Figure 4.2.2: Close-up of wrinkles in a biofilm. In this fluorescence composite image, the center of the colony, at the bottom left, is red from the high proportion of motile cells (red). Although much of the rest of the colony has sporulated (green), channels underneath the radial wrinkles could bring in nutrients from the perimeter of the colony to the center.

switching from matrix production to spore formation.

4.3 Nutrient concentration profiles

Since these changes in gene expression are likely at least partially the result of nutrient depletion, we measure the concentrations of glycerol and glutamate

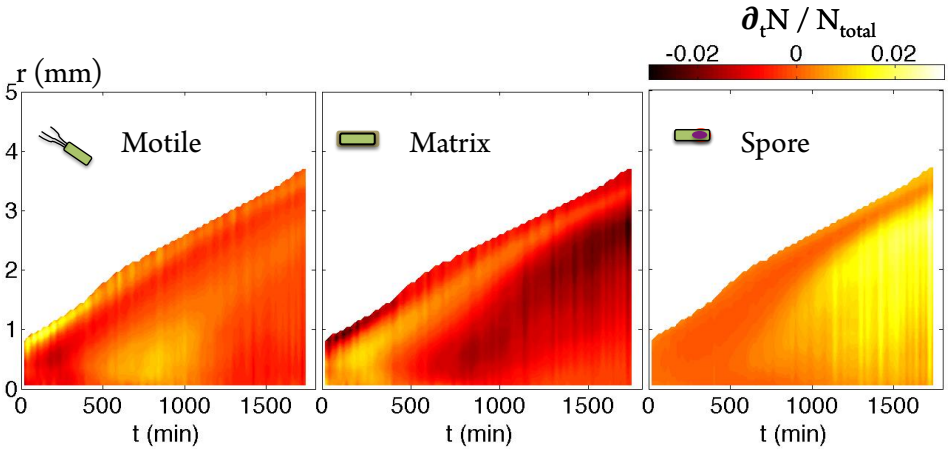

Figure 4.2.3: Spatiotemporal plots of changes in gene expression. These plot shows time derivatives for each of the fluorescence channels. Darker colors indicate a decrease in the fraction of the total population and lighter colors indicate an increase. The magnitude of these changes is on the order of several percent per 20 minute time step.

directly underneath the colony over time and for different initial nutrient concentrations. An enzymatic assay allows measurement of both glycerol and glutamate. Both appear to be consumed at the same rate, so we focus only on glutamate.

Nutrients are depleted faster from the agar than can be replenished by diffusion, leading to a region of depletion underneath the colony that increases over time, as shown in Fig. 4.3.1. The position of the peak of matrix production is correlated to the depletion of nutrients. Sporulation occurs closer to the center of the colony, where these concentrations are even lower. Although these patterns are consistent with cells producing matrix, then sporulating, in response to starvation, Chapter 5 shows how to test whether a specific threshold can explain these transitions or some type of chemical signaling is also required.

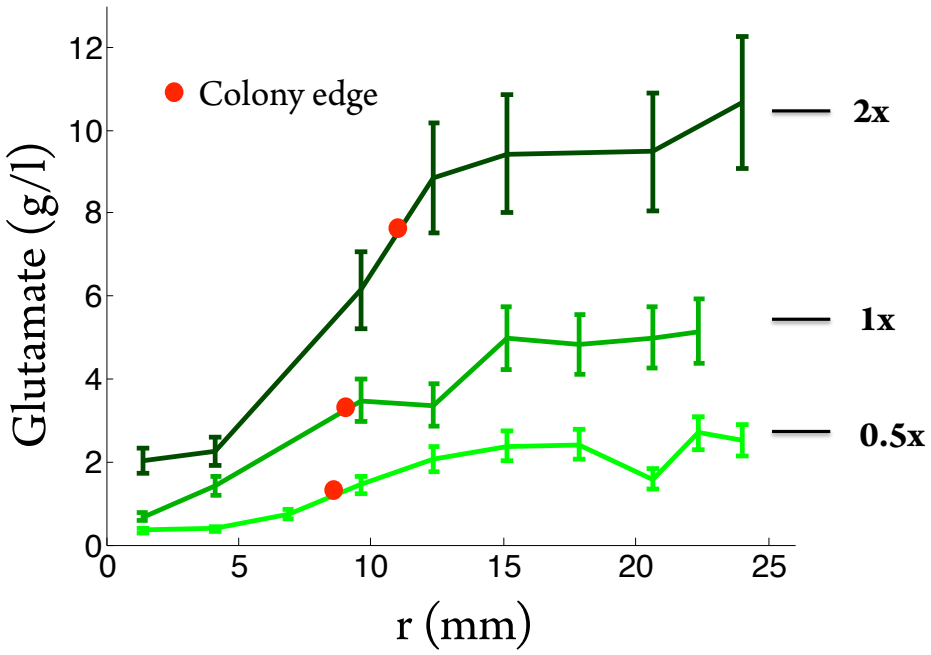

Figure 4.3.1: Depletion of nutrients in agar. Radial profiles of glutamate concentration are shown for three different initial concentrations of nutrients, taken from agar underneath a 48 h old colony. In each case, the concentration underneath the center of the colony decreases over time, and the region of depletion extends outside the perimeter of the colony, which is denoted by the red dot.

4.4 Effect of nutrient levels on gene expression

To further investigate the connection between nutrients, signals, and gene expression, we grow biofilms under different initial concentrations of nutrients. Five colonies each grow on agar plates with 0.5x (2.5 g/l glycerol and 2.5 g/l glutamate), 1x (5 g/l glycerol and 5 g/l glutamate), and 2x (10 g/l glycerol and 10 g/l glutamate) the normal concentration. Although MSgg contains many nutrients, these two are the primary carbon and nitrogen sources for the biofilms. The colonies grow in a 30 °C incubator. We remove the colonies every 8 hours for microscope observations; the total duration of the experiment is 72 hours.

The nutrient concentrations have a consistent effect on the future growth of

the biofilms. Higher nutrient levels lead to larger, thicker colonies. These colonies have higher populations of both motile and matrix producing cells, and sporulation is delayed. These results are consistent with the sporulation process being triggered by nutrients falling below a specific threshold. Spatiotemporal plots that summarize our results are shown in Fig. 4.4.1.

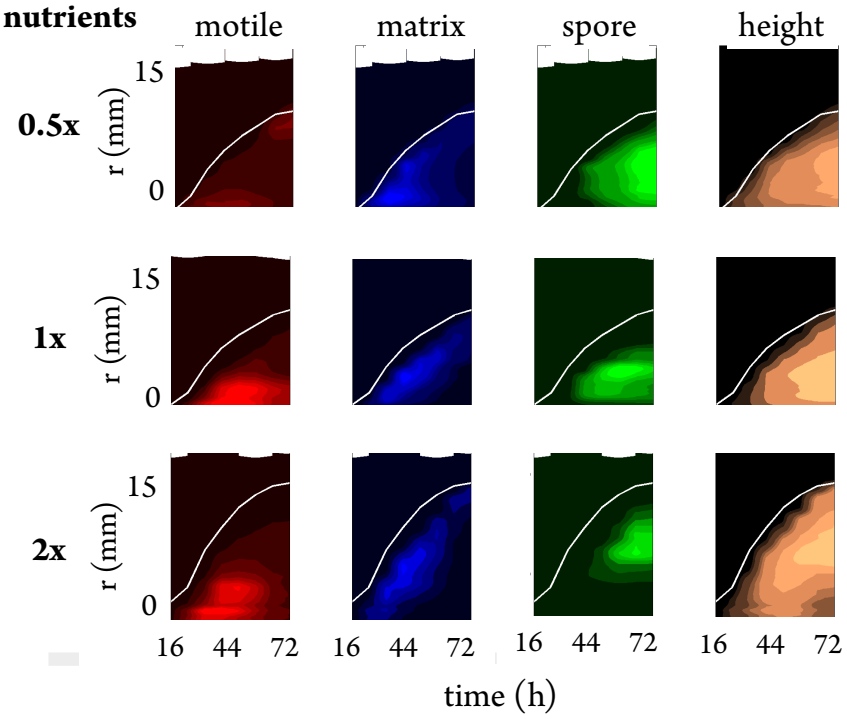

Figure 4.4.1: Gene expression patterns for different nutrient levels. For each image of a biofilm, we find the center and azimuthally average the intensity of the fluorescence and transmitted light signals. We track three colonies at different nutrient concentrations. Each row corresponds to a different nutrient concentration: 0.5x, 1x, and 2x the standard glycerol and glutamate concentration in MSgg. Each column corresponds to a different fluorescence channel. Within each plot, the x-axis is time and the y-axis is the radial position. The intensity corresponds to the intensity of the fluorescence signal or to the height of the colony. The white line indicates the approximate radius of the colony.

The spatiotemporal plots are a valuable tool for exploring trends in phenotype sub-populations under different growth conditions. However, to understand

phenotype switching requires measurements of the growth rates of the colony, since the growing biofilm is a moving frame of reference. Since the profiles of gene expression vary along the radial direction, outward expansion of the colony would lead to a change in the measured value at a fixed point. In addition, cell division causes the motile and matrix-producing populations to increase, while the sporulating cell population would stay fixed in the absence of switching between phenotypes.

The next chapter explains a more comprehensive approach to measuring transition rates between phenotypes in a growing biofilm, by taking into account the growth rates.

5

Calculation of Transition Rates between Phenotypes

How do bacteria in a colony decide when to switch between phenotypes? We address this question using a combination of spatiotemporal information about gene expression from the previous chapter, along with measurements of the expansion rate of the colony and nutrient levels underneath the colony. Numerical simulations complement our observations and allow us to estimate nutrient levels with greater spatial and temporal resolution. These simulations help test assumptions about whether changes between phenotypes are due to nutrients alone, or require some type of chemical signaling.

5.1 Measurement of growth rates

Since the biofilm grows over time, we need to convert from a reference frame relative to the growing colony to the stationary reference frame of the agar plate. The height profiles $h(r,t)$ from the transmitted light images allow determination of growth rates: $u(r,t)$ is the average rate of horizontal expansion and $g(r,t)$ is the average rate of cell division, both of which vary along the radial position. The biofilm can be viewed as a fluid which flows with a flux $q = uh$. Volume conservation then reads:

$$\frac{dh}{dt} = \frac{1}{r}\frac{\partial\,(rq)}{\partial r} = gh. \tag{5.1}$$

The simplest curve $u(r)$ compatible with the boundary conditions $u(r=0,t)=0$ and $u(r=R,t) = (\partial R(t)/\partial t)$ is a linear function: $u(r,t) = (\partial R(t)/\partial t)\,(r/R)$.

Inverting the volume conservation relation, we can solve for g:

$$g = \frac{1}{h}\frac{\partial h}{\partial t} + \frac{u}{r} + \frac{\partial R/\partial t}{R} + \frac{u}{h}\frac{\partial h}{\partial r}. \tag{5.2}$$

The growth rates can be calculated numerically from finite differences of the height profiles in space and time. The height profiles, time derivatives, radial derivatives, and velocity function for a representative biofilm are shown in Fig. 5.1.1. The growth rate is dominated by the horizontal expansion term u/r, which is an order of magnitude larger than the other two terms.

By applying Eq. 5.2 we obtain the spatiotemporal plot shown in Fig. 5.1.2. The growth rate in the early stages of the biofilm is close to $5 \cdot 10^{-3}\mathrm{min}^{-1}$; this growth rate persists along the perimeter of the colony for most of the remaining time, until it starts to decline at the end.

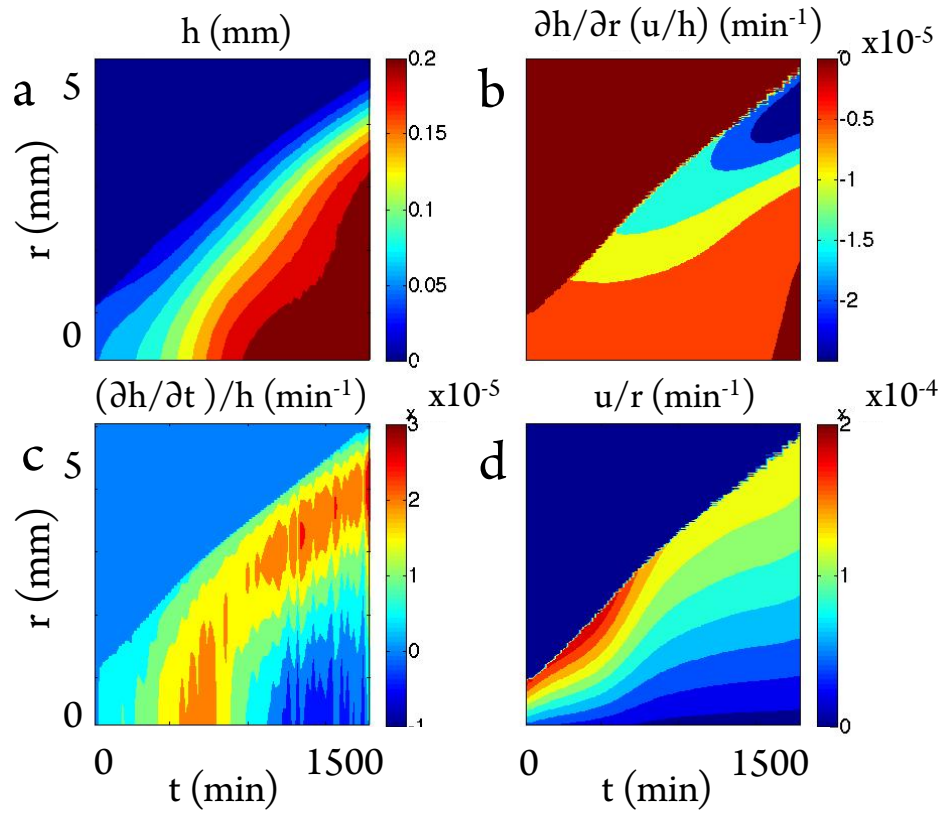

Figure 5.1.1: Derivatives of height profiles. The first step towards calculating the growth rate and phenotypic transition rates is determination of spatial and radial derivatives. Each plot shows the radial position along the y-axis and the age of the colony on the x-axis. a) height profiles, b) radial derivative, c) time derivative, and d) outward velocity. The derivatives are scaled so that b) – d) have units of min^{-1}.

Verification with constitutive fluorescence

We verify this method by analyzing a colony from a constitutively-labeled strain, in which all the cells fluoresce. If the number of cells is proportional to the height of the colony, then at every pixel fluorescence intensity would be related to the local height by a constant. However, the presence of non-fluorescent, sporulated cells leads to a lower intensity. Although we have preliminary results with a strain that constitutively expressed the red fluorescent protein, future work will check

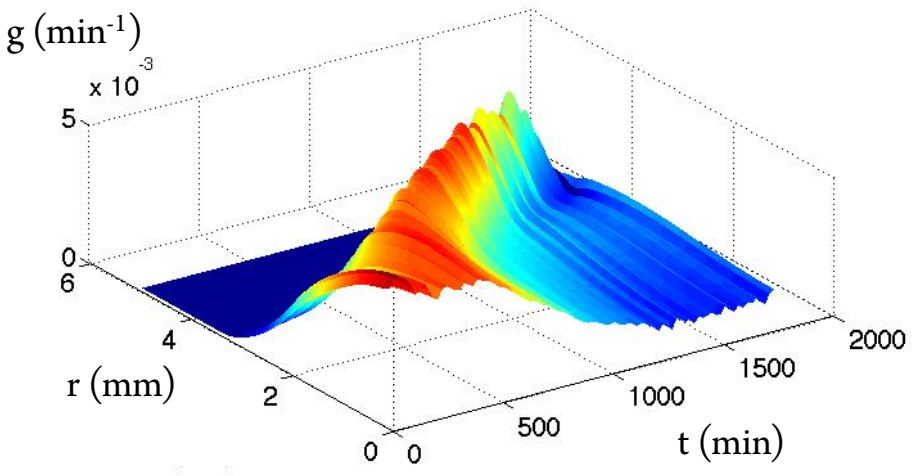

Figure 5.1.2: Spatiotemporal plot of growth rate. The left axis is the radial position, the right axis is time, and the z-axis is the local growth rate. The growth rate is far larger at early times and along the edge of the colony as the biofilm grows.

other fluorophores.

5.2 Determination of transitions between phenotypes

To determine transition rates between phenotypes, rather than just populations, we must adjust for the effect of expansion of the colony. If the total population and volume of the colony were constant, then transitions could be calculated entirely from the changes in fluorescence intensity. However, in an intact colony, the population and size change, which also affects the fluorescence intensities. The large magnitude of the advection term u/r shows that future experiments must take into account the expansion of the colony.

5.2.1 Mathematical model for phenotypic switching

We develop a model to allow us to infer cell type switching rates from the fluorescence rates, as a function of both space and time. The sub-population of each phenotype is denoted by n_i where $i = 1, 2, 3,$ and4 correspond to motile,

matrix-producing, sporulating, and non-fluorescent cells. The motile and matrix producing cells divide after a doubling time
$g^{-1} = \tau\,(n_1 + n_2)\,/\,(n_1 + n_2 + n_3 + n_4)$. The transition rates are denoted by the subscripts: A_{12} is the rate at which cells switch from motile to matrix producing, A_{23} is the rate at which cells switch from matrix producing to sporulating, and A_{34} is the rate at which sporulating cells stop fluorescing. The master equations to describe all the phenotype populations are:

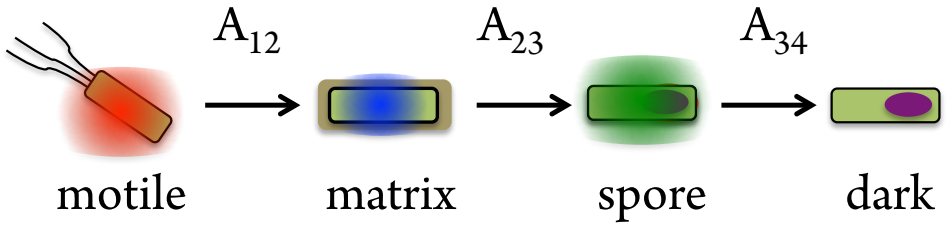

Figure 5.2.1: Definition of transition rates. Motile cells become matrix producing cells at a rate A_{12}, matrix producing cells become spore forming cells at a rate A_{23}, and sporulating cells stop fluorescing at a rate A_{34}.

$$\frac{\partial n_1}{\partial t} + \frac{1}{r}\left[rq_1\right]_r = -A_{12}n_1 + \frac{n_1}{\tau} \tag{5.3}$$

$$\frac{\partial n_2}{\partial t} + \frac{1}{r}\left[rq_2\right]_r = A_{12}n_1 - A_{23}n_2 + \frac{n_2}{\tau} \tag{5.4}$$

$$\frac{\partial n_3}{\partial t} + \frac{1}{r}\left[rq_3\right]_r = A_{23}n_2 - A_{34}n_3 \tag{5.5}$$

$$\frac{\partial n_4}{\partial t} + \frac{1}{r}\left[rq_4\right]_r = A_{34}n_3 \tag{5.6}$$

$$\tag{5.7}$$

With this model, we aim to infer A_{12} and A_{23} as a function of space and time. The rate of fluorescence decay A_{34} is found independently from the constitutively-labeled strains. The transitions are illustrated in Fig. 5.2.1.

Using finite difference methods, we calculate each of the derivatives in Eq. 5.3

– 5.5 and solve for A_{12} and A_{23}. To ensure that the computed transition rates are meaningful, we compare the magnitude to each of the other terms in the equation.

5.3 Modeling cell transitions

Our data suggest several plausible models for transition rates. The simplest scenario is one in which the cells switch from being motile to producing matrix below a nutrient threshold of c_1 and switch from producing matrix to forming spores below a second nutrient threshold c_2. In the simplest case, both of these rates are proportional to a coefficient A_0.

$$A_{12} = 0 \quad c > c_1 \tag{5.8}$$

$$A_{12} = A_0/\tau \quad c < c_1 \tag{5.9}$$

$$A_{23} = 0 \quad c > c_2 \tag{5.10}$$

$$A_{23} = A_0/\tau \quad c < c_s \tag{5.11}$$

To test the validity of this model, we compare spatiotemporal maps of the transition rates to the simulated nutrient values in the agar substrate. If the iso-nutrient lines match one of the transition rates, then the transition can be explained in terms of nutrients. Preliminary results suggest this model holds true for the transition to sporulation, but not the transition to matrix production.

Current studies are exploring the spatiotemporal growth patterns at high temporal resolution for a range of initial nutrients. With this information, we will be able to check whether the transitions between phenotypes are described by Eq. 5.8. If the nutrient levels are not sufficient, we can compare against simulated signal calculations, computed with the Eqs. A.6 – A.10.

The next section shows how numerical simulations can complement the nutrient concentration experiments described in the previous chapter, for more accurate comparison with the phenotypic switching maps.

5.4 Modeling nutrients

5.4.1 Calculation of nutrient concentrations

Since it is not feasible to measure the nutrient concentrations every 20 minutes, we model the flow of nutrients to estimate the values for intermediate times and locations.

Since the biofilm is much thinner than the agar, we approximate the distribution of nutrient in the biofilm with its quasi-steady solution. This allows us to simulate the agar alone and greatly speed up the numerical simulations. We impose consumption through a flux condition at the agar/biofilm interface.

In our simulation, the initial condition is a uniform initial concentration c_∞ everywhere in the agar. As the simulated biofilm grows, the size of the sink at the top surface expands to match its radius. For the present simulation, we assume a constant rate of consumption throughout the biofilm. The nutrients flow by diffusion, with a diffusion constant of $D = 10^{-5}\text{cm}^2/\text{s}$, corresponding to glycerol in water. The following set of differential equations and boundary conditions corresponds to the full set of equations used in the simulation:

$$
\begin{aligned}
c_t &= D\left(c_{zz} + c_{rr} + \frac{c_r}{r}\right) - \Gamma\frac{c}{c^* + c} && (5.12)\\
c(t=0) &= c_\infty && (5.13)\\
c_z(z=0) &= 0 && (5.14)\\
c_z(z=L+h) &= 0\,(\hat{n} \approx \hat{z}) && (5.15)\\
c_r(r=W) &= 0 && (5.16)\\
c_r(r=0) &= 0. && (5.17)
\end{aligned}
$$

where we have modeled the nutrient consumption through the customary Monod model, in which cells eat at a rate Γ when nutrients are abundant and at a rate $\approx \Gamma\,(c/c^*)$.

We obtain the quasi-steady state solution for the biofilm by neglecting the

horizontal gradients and time derivatives:

$$c_{zz} = \frac{\Gamma}{D}\frac{c}{c+c^*} \tag{5.18}$$

$$c(z=h) = 0 \tag{5.19}$$

The solution reads:

$$\begin{array}{rcll} c & \approx & c_0 - \gamma\left(\zeta - \frac{\zeta^2}{2}\right) & c > c^* \\ c & \approx & c_0 \frac{\cosh\left(\sqrt{\gamma/c^*}(1-\zeta)\right)}{\cosh\left(\sqrt{\gamma/c^*}\right)} & c < c* \end{array} \tag{5.20}$$

where $\zeta = (L/h)$, so that if L is the thickness of the biofilm $\zeta = 0$ is the biofilm/agar interface.

Here c_0 is the concentration of nutrients at the interface, and is determined by continuity across the boundary. The flux from the agar to the biofilm can then be calculated by simply differentiating in z in this quasi-steady state solution: $-D\,(\partial c/\partial z)$. We will use the flux to impose the boundary condition at the biofilm/agar interface, as described in the next section.

5.4.2 Numerical simulation

We use the `ode15s` solver in Matlab to solve the long-time asymptotic solution for each point throughout the agar, using the quasi-steady state approximation for the biofilm. In order to resolve scales ranging from tens of microns to centimeters, we need hundreds of grid points.

We non-dimensionalize the system by the dimensions of the petri dish and the initial concentration of nutrients, so that $\varepsilon \to L/W, r \to r/W, z \to z/L$, and $c \to c/c_\infty$. The partial differential equation for nutrient diffusion can now be written as:

$$c_t = c_{zz} + \varepsilon^2\left(c_{rr} + \frac{c_r}{r}\right). \tag{5.21}$$

The boundary conditions are:

$$c_z(z=1) = \frac{L}{h} c_\zeta^{\text{biofilm}}(\zeta=0) \tag{5.22}$$

$$c_z(z=0) = 0 \tag{5.23}$$

$$c_r(r=1) = 0 \tag{5.24}$$

$$c(t=0) = c_\infty \tag{5.25}$$

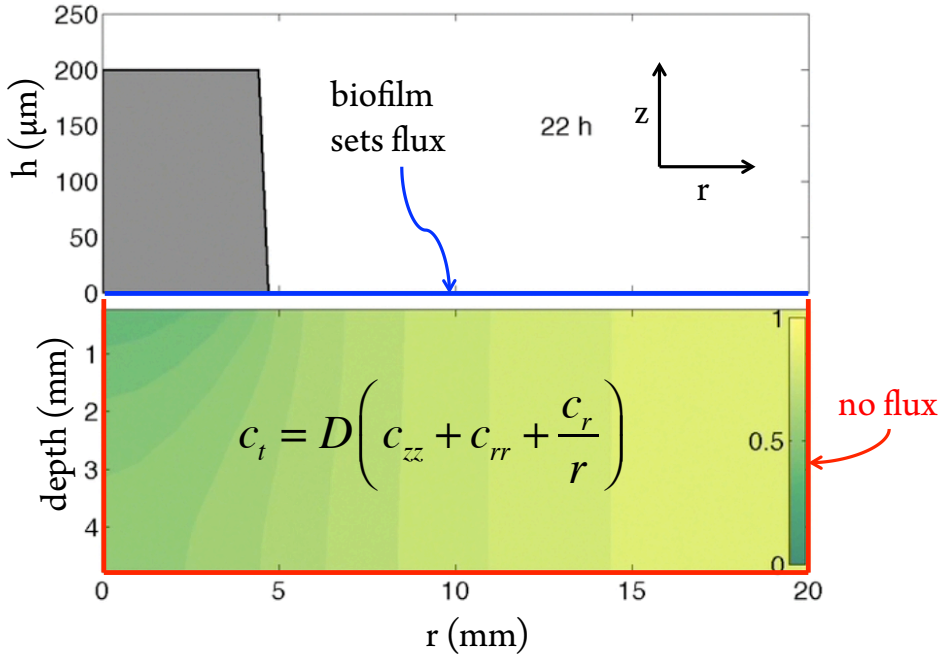

Figure 5.4.1: Numerical simulation of nutrient concentrations. We solve the diffusion equation throughout the volume of the agar substrate. The bottom, center, and outer boundary conditions are set to zero flux and the upper boundary condition is set by the nutrient consumption by the biofilm.

Table 5.4.1 shows the parameters used in the simulation. The consumption rate of bacteria is based on the following assumptions: the mass of a *Bacillus subtilis* cell is 150 fg, the division time in a colony is about one hour, and the dry

mass fraction is 20%, so the consumption rate is 30 fg/h (glucose *E. coli*, K_s = (30 micrograms to 5 mg)/L) [38]. In future experiments, this value will be tuned to match experimental nutrient concentration profiles.

Table 5.4.1: Physical parameters

Symbol	Quantity	Value
R	petri dish radius	44 mm
L	agar depth	5 mm
Γ	nutrient consumption rate	0.02 mM/s
c_∞	initial nutrient level	5 mM
$c^\star$	starvation threshold	$0.01c_\infty$

The spatiotemporal plot in Fig. 5.4.2 shows the simulated nutrient concentrations directly below the biofilm. The radius of the colony in the simulation increases at a constant rate from 1 to 4 mm. As expected, the concentration underneath the center of the colony decreases over time and the region of nutrient depletion extends outside the perimeter of the colony. The consumption rate will be matched to experimental height profiles in future simulations.

We overlay the iso-nutrient lines on the spatiotemporal plots of the time derivatives of the sub-populations of phenotypes (Fig. 5.4.3). This allows us to easily see any correlations between nutrient levels and changes in sub-populations. The increase in the sub-population of sporulating cells lies within one of the iso-nutrient lines, suggesting that it is triggered when nutrients fall below a threshold level. The motility and matrix production show no correlation with the iso-nutrient lines, suggesting that some other mechanism is responsible for the transition between them. These proportional changes in fluorescence ($\approx 10^{-2}$) are larger than the growth rates of the colony ($\approx 10^{-3}$), but future analysis will more rigorously account for the expansion of the colony.

The mathematical framework for studying the effect of nutrients on biofilm

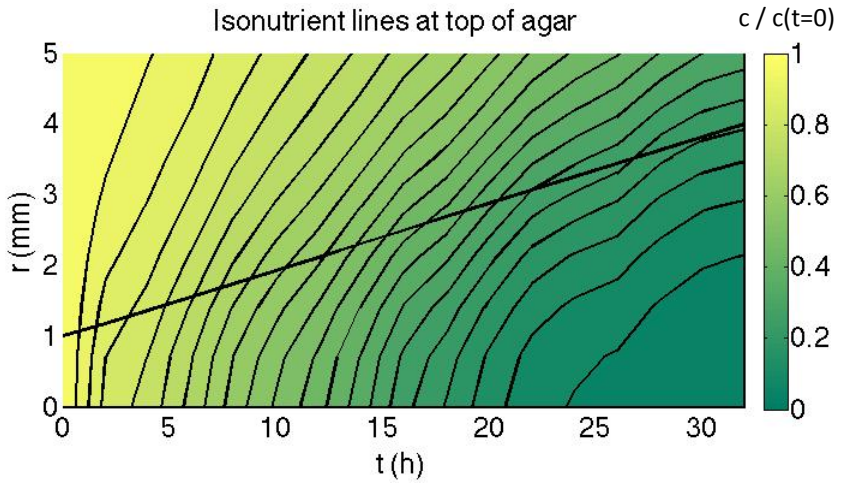

Figure 5.4.2: Spatiotemporal plot of simulated nutrient concentrations. The color scale ranges from yellow to green to denote the nutrient concentrations. The diagonal black line indicates the radius of the colony during the simulation. The blue lines are iso-nutrient lines, corresponding to a constant nutrient concentration.

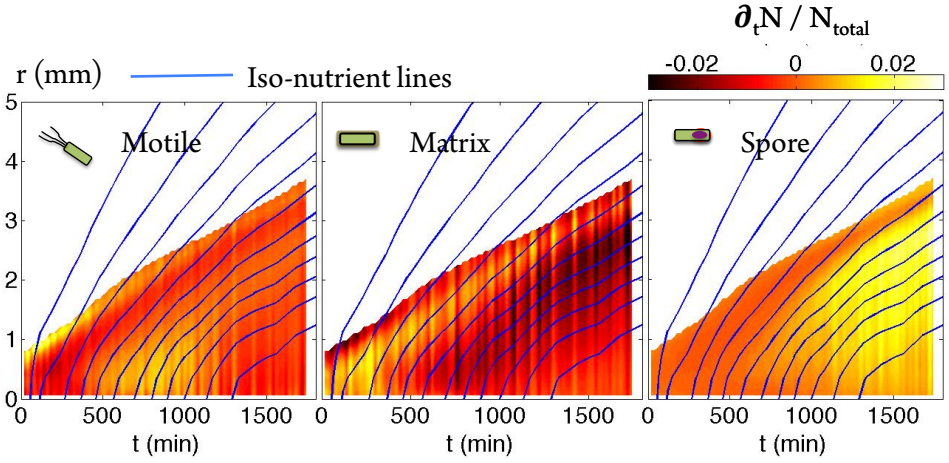

Figure 5.4.3: Overlay of iso-nutrient lines on spatiotemporal plot of changes in subpopulations of phenotypes. The initiation of the rise in sporulation occurs at the same location as one of the iso-nutrient lines, but the changes in the expression of motility and matrix production show no such correlation.

development is similar to that for chemical signals. The governing equations and boundary conditions are described in the Supplementary Information in Eq. A.6 – A.10. Future work will investigate whether the signaling molecules can explain the transition to matrix production.

6

Future Applications

This approach to quantifying the development of sub-populations of phenotypes in *Bacillus subtilis* is broadly applicable to other microbial systems. The two necessary steps are to fluorescently label the relevant phenotypes and to characterize the optical properties of the biofilm. This allows conversion of fluorescence microscope images to sub-populations of each phenotype. By simultaneously tracking the growth rate of the colony, using transmitted light images, the material derivate for the changes in sub-population is calculated, rather than just the time derivative at each location. By taking into account the growth, the transition rates between phenotypes can be calculated.

With a spatiotemporal map of phenotype transition rates, we look for correlations with environmental parameters, such as nutrient levels. Preliminary results demonstrate the feasibility of this approach and a natural extension is to repeat the measurements for a range of nutrient conditions. Although

sporulation seems triggered by a decrease in glycerol and glutamate concentrations, additional experiments would quantify the threshold concentration and elucidate the role of other factors, such as chemical signalling.

While working to demonstrate the feasibility of the technique to explore the sporulation pathway in *Bacillus subtilis*, we came across several potential extensions that could lead to future research projects. Below are some of the most promising avenues to explore.

6.1 Improved measurements of growth rates

More accurate maps of the growth rates of the colonies would lead to more accurate calculations of phenotype transition rates. Beads can be sprinkled on the surface to measure the local strain field across the surface of the colony. We tested the feasibility of this idea with 100 μm diameter polystyrene beads, as shown in Fig. 6.1.1; in future experiments, fluorescent beads on unlabeled colonies may yield more accurate results. Stereo imaging is another potentially useful technique; three-dimensional information about the surface morphology would be the most accurate way to find the growth rate.

6.2 Observations of individual cells in micro-colonies

Although we studied macroscopic colonies, cell transitions could be directly observed with micro-colonies. Existing protocols for growing monolayer colonies on agar pads [39] could be adapted for this technique. This would have the advantage of no longer requiring correction for the attenuation of the biofilm material.

6.3 Explorations of other microbial systems

This method could be applied to numerous other biofilm systems. Labeled versions of mutant *Bacillus subtilis* strains could yield further insight into the

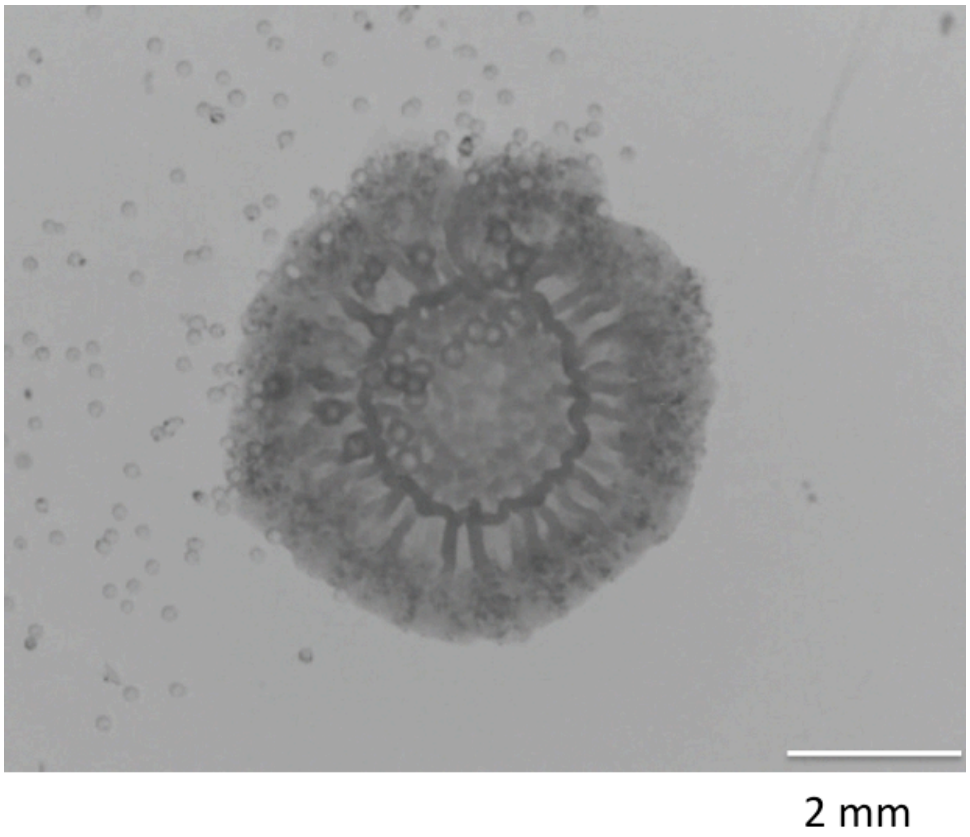

Figure 6.1.1: Tracking local displacements with beads. 100 μm diameter polystyrene beads are sprinkled on half of an agar plate immediately after spotting a colony. The displacements of the beads as the colony grows show the local displacement field.

structure and timing of sporulation. Matrix knockouts do not produce wrinkles, providing an easy way to tell whether channels are allowing nutrients to flow to the centers of the colonies.

Strains labeled for surfactin or other intercellular signal molecules could elucidate the dynamics of cellular communication during biofilm development. Labeling surfactin in *Bacillus subtilis* has not been feasible so far, but analogous labels are available in *Pseudomonas*.

Eventually, this method could be used to suggest new mechanisms for phenotypic switching in multi-species biofilms.

A

Supplementary Information

A.1 Table of strains constructed

All strains were based on the 3610 WT Strain of *Bacillus subtilis*. The first three strains, HV1161, ZK3664, and HV1133, were provided by Hera Vlamakis from the Kolter Lab. The remaining strains were provided by Matt Cabeen from the Losick Lab, using the 3610 strain from James Wilking. Matt constructed three constitutively labeled strains: MTC822 (red), MTC824 (citrus), and MTC828 (green). He also constructed three single labeled strains, MTC826, MTC830, and MTC832, one for each phenotype. These were used to make the double labeled strain, MTC834, and finally the triple labeled strain, MTC836. The gene for the spore forming reporter was linked to an alternate amyE locus, to avoid interference with the matrix reporter.

Table A.1.1: Strains

Strain	Genotype	Antibiotic
HV1161	*lccA::PsspB-yfp / amyE::Pyqxm-cfp*	spec
ZK3664	*amyE::PsspB-yfp*	spec
HV1133	*amyE::PskfA-yfp*	spec
MTC822	*amyE::Phyperspank-mKate2*	chlor
MTC824	*ywrK::Phyperspank-citrus*	chlor
MTC826	*sacA::Phag-mKate2*	kan
MTC828	*amyE::Phyperspank-GFP*	chlor
MTC830	*amyE::PsspB-citrus*	chlor
MTC832	*amyE::PtapA-CFP*	spec
MTC834	*sacA::Phag-mKate2 amyE::PtapA-CFP*	kan, spec
MTC836	*sacA::Phag-mKate2 amyE::PtapA-CFP amyE::PsspB-citrus*	kan, spec, chlor

A.2 Elaboration of mathematical theory

A.2.1 Explanation of growth model

We describe the expansion of the biofilm due to cell division by the continuity equation, which links the vertical growth rate, g, and horizontal velocity, u, to the height profile, $h(r,t)$.

For a regular fluid, like water, the volume is conserved, so the equation is given by:

$$h_t = -(uh)_r \tag{A.1}$$

For a growing biological material, the height increases at a rate, g, so without horizontal expansion, the height would increase by:

$$h_t = gh \tag{A.2}$$

These two effects of growth and horizontal expansion are added together to

obtain the continuity equation:

$$h_t + (uh)_r = gh \tag{A.3}$$

.

A.2.2 Chemical signaling

The mathematical framework for studying the effect of nutrients on biofilm development is similar to that for nutrient levels. We model a field s representing a concentration of a signaling molecule, instead of the nutrient concentration c. The molecule is produced at a rate $\Gamma_s \frac{c}{c^* + c}$ and consumed at a rate $\frac{s}{\tau^D}$.

$$\begin{aligned} s_{\zeta\zeta} &= \Gamma_s \frac{c}{c^* + c} + \frac{s}{\tau^D} && \text{(A.4)} \\ s_\zeta(1) &= 0 && \text{(A.5)} \end{aligned}$$

We can non-dimensionalize the system in the same manner as before: $s' = s/c_\infty, \gamma_s(r) = \Gamma_s h^2(r)/(Dc_\infty), \tau'(r) = \tau^D/h^2, z' = z/L, r' = r/W$, and $\varepsilon = L/W$. After omitting the primes, we obtain the following set of equations for both nutrients and signaling molecules:

$$\begin{aligned} c_t &= c_{zz} + \varepsilon^2 \left(c_{rr} + \frac{c_r}{r} \right) && \text{(A.6)} \\ s_t &= s_{zz} + \varepsilon^2 \left(s_{rr} + \frac{s_r}{r} \right) && \text{(A.7)} \\ c_z(0) &= s_z(0) = 0 && \text{(A.8)} \\ c_z(1) &= \frac{L}{h} c_\zeta(0) && \text{(A.9)} \\ s_z(1) &= \frac{L}{h} s_\zeta(0) && \text{(A.10)} \end{aligned}$$

B

The Kitchen as a Physics Classroom

B.1 Abstract

Cooking is a tangible, familiar, and delicious tool for teaching physics, which is easy to implement in a university setting. Through our courses at Harvard and UCLA, each year we are engaging hundreds of undergraduate students, primarily non-science majors, in science concepts and the scientific research process. We find that weekly lectures by chefs and faculty, paired with edible lab experiments, generate enthusiasm and provide strong motivation for students to learn physics. By the end of the course, students are able to conduct independent scientific research and present their results in a final science fair. Given the considerable broad appeal of food and cooking, the topic could be adapted to other post-secondary as well as secondary-level courses.

B.2 Introduction

A major challenge in teaching physics is to make students see the connection to their everyday lives. In many physics courses, concepts are presented using abstract examples, such as stretching an ideal spring or heating a copper rod. To make the material more relevant, we developed a curriculum that uses examples from cooking to teach physics concepts to undergraduate students. The resulting course, "Science and Cooking: From Haute Cuisine to Soft Matter Science," fulfills the Science of the Physical Universe requirement as part of the new General Education program at Harvard. Courses that fulfill this requirement are designed for non-science majors and must connect lessons to students' lives outside the classroom and beyond their college years. The curriculum was subsequently adapted at UCLA where "Science and Food: The Physical and Molecular Origins of What We Eat" fulfills the Physical Sciences requirement of the General Education program.

Cooking provides a rich set of examples to introduce topics in the physical sciences. Nearly all cooking involves irreversible physical or chemical transformations that are intended to improve some combination of the texture, flavor, and nutritional content of a food. One especially versatile example is the egg: heating can transform the whites into an opaque gel, whisking can turn the whites into a foam, and blending the yolks with olive oil and lemon juice can produce the stable emulsion known as mayonnaise. However, even a small variation in method or technique can result in cooked eggs that are rubbery, foams that collapse, or emulsions that break. In general, the success or failure of a dish can be explained by a small number of scientific concepts, such as elasticity and diffusion, which are commonly discussed in introductory physics courses.

Cooking also serves as a familiar and tangible example of the scientific method. Each recipe is an experiment; deviating from tradition can result in culinary disaster. Like a scientist, the intrepid cook can explore a range of variations in ingredients and methods through careful experimentation and documentation: systematically varying one parameter of the recipe at a time and observing the

outcome. Knowledge of scientific concepts can help to prioritize which of these parameters would be most useful to vary. For example, knowledge of heat diffusion can show how long to cook a molten chocolate cake [40] (Fig. B.2.1).

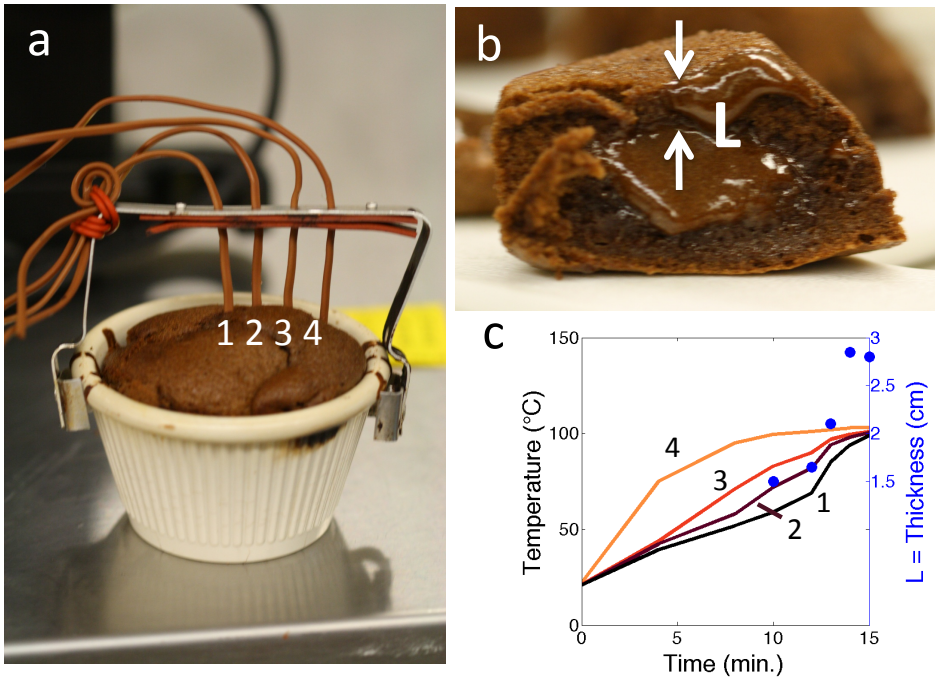

Figure B.2.1: Molten chocolate cake as an example to teach heat transfer. a) Thermocouples are used to measure the rise in temperature at different points inside the cake as it bakes in an oven. b) The thickness, L, of the solid crust of the cake increases over time. c) Experimental data for the rise in temperature and thickness show how heat flows from the outside towards the center of the cake.

In addition to using everyday examples, like an egg, recent developments in high-end restaurants provide new educational opportunities. Over the past several decades there has been a revolution in the kitchens of many restaurants, inspired by methods from scientific laboratories [41], [42], [43] . Pioneers such as Ferran Adrià (el Bulli) and Heston Blumenthal (The Fat Duck) produce striking culinary creations especially suited for teaching science. For example, Joan Roca (El Celler de Can Roca) uses precise regulation of temperature,

enabling unprecedented control over protein denaturation and the final texture of the food [44]. As another example, polymers facilitate the creation of novel food textures; instead of using egg whites or dairy fat to stabilize a foam, only a small amount of the naturally occurring surfactant lecithin can create similar textures of foams that have more pure flavors. These chefs are also famous for their use of liquid nitrogen, rotary evaporation, centrifugation, and other techniques more commonly associated with scientific laboratories.

B.3 Course structure

Our aim is to create a physics class for non-scientists, assuming a background of basic high school chemistry and physics. We seek to engage students in scientific concepts and methods by showing them the science underlying the food of both haute cuisine and everyday cooking. Although several existing courses focus on chemical aspects of food [45], [46], resources that highlight the physics of cooking are sparse [40], [47]. Moreover, despite the central importance of soft matter physics in cooking, topics such as gels, foams, and emulsions are rarely taught at an introductory college level. For these reasons, we present here our own curriculum where the physics of soft materials is central. In addition to physics concepts, chemical reactions and microbial growth are also essential for understanding fundamental culinary processes, such as browning and fermentation; therefore, we additionally include these concepts in our curriculum.

B.3.1 Overview of Curriculum

To teach this coherent curriculum focusing on soft matter science, we devised a tight pedagogical structure. Each week focuses on a single scientific idea that is essential to numerous culinary examples. This idea is introduced through the "Equation of the Week" (Table B.3.1), then elaborated through lectures by faculty and chefs, as well as a recipe prepared by the students during their lab section.

Table B.3.1: Equations of the Week: Each week students are presented with an equation and a recipe, to accompany the demos from the visiting chefs and the science explanations from the course instructors. Guide to symbols: Q = heat applied, m = mass, c_p = specific heat, ΔT = change in temperature, U_{int} = molecular interaction energy, k_B = Boltzmann constant, C = empirical constant, T = temperature, E = elasticity, l = cross-link spacing, L = distance of diffusion, D = diffusion constant, t = time elapsed, T_{in} = initial temperature inside food, T_{out} = temperature at outside boundary of food, τ_{o} = heating time constant, L_{o} = distance to center of food, η = viscosity, τ_{flow} = time scale for material to flow, σ = surface tension, R = radius of droplets or bubbles, φ = volume fraction, φ_c = critical volume fraction, NaHCO_3 = sodium bicarbonate, AcidNa = acid with extra sodium, AcidH = acid with extra hydrogen, H_2O = water, CO_2 = carbon dioxide, N = number of microbes in the population, N_{o} = initial count of microbes, k = microbial growth constant, τ_2 = microbial doubling time.

Week	Scientific Concept	Equation of the Week
1	Energy, temperature, and heat	$Q = m\, c_p\, \Delta T$
2	Phases of matter	$U_{\text{int}} = C\, k_B\, T$
3	Elasticity and gels	$E = \frac{k_B\, T}{l^3}$
4	Diffusion	$L = \sqrt{4D\, t}$
5	Heat transfer	$T(t) = (T_{\text{in}} - T_{\text{out}})\, e^{-t/\tau_{\text{o}}} + T_{\text{out}}; \tau_{\text{o}} = \frac{L_{\text{o}}^2}{4D}$
6	Viscosity and polymers	$\eta = E\, \tau_{\text{flow}}$
7	Emulsions and foams	$E = \frac{\sigma}{R}\left(\varphi - \varphi_c\right)$
8	Chemical reactions	$\text{NaHCO}_3 + \text{AcidH} \rightarrow \text{AcidNa} + \text{H}_2\text{O} + \text{CO}_2$
9	Microbes	$N(t) = N_{\text{o}} e^{k\, t}; k = \ln 2/\tau_2$

1. **The Equation of the Week summarizes each scientific concept**: To provide a rational framework for understanding the nine concepts we identified as relevant to cooking, we select a single equation for each concept that summarizes the connection between the observable aspects of a food and its microscopic structure. For instance, during the week on heat transfer, the Equation of the Week (#4 in Table B.3.1) relates the heat diffusion into a material, L, such as indicated by the solidification of the outer layer of the molten chocolate cake, to the heat diffusion constant, D, and the cooking time, t, (Fig. B.2.1). While many of the equations we present are exact for ideal systems, food systems are complex; in the case of the cake, water evaporation from the surface, changes in the heat

diffusion constant during solidification, and other factors could affect the heat flow. We find that the students appreciate a discussion highlighting the limitations of the equations, and the extent to which they can provide a good approximation.

2. **Lectures feature both chefs and professors**: Course instructors give science lectures based on the Equation of the Week, which include derivations, worked example problems, and demonstrations. In addition, each week features a culinary lecture by a visiting chef; these lectures complement the corresponding science lectures, to reinforce the science concepts. For example, during the week covering heat transfer, the course staff bakes a cake, plots the rising internal temperature in real-time, and introduces the heat diffusion equation (#4 in Table B.3.1). The corresponding guest lecture shows how heat transfer is applied to chocolate tempering. Chefs provide tangible examples of the scientific concepts; these live demonstrations, often involving food samples, are popular among students.

3. **Lab sessions involve experiments with food**: Weekly labs give students a hands-on opportunity to explore the current science concept and apply the Equation of the Week. Lab sessions are designed to last a total of two hours, with the first thirty minutes devoted to a review of the lectures and guided problem solving. In conducting their laboratory investigations, students work in groups of three to collect data, record observations, as well as analyze and eat their results. Such tactile lab exercises are an ideal way to engage students who may have diverse learning styles [48]. Moreover, inquiry-based approaches to lab instruction are effective methods to foster conceptual understanding and scientific reasoning [49]. The labs also guide students on how to vary a single parameter in an experiment, in order to obtain a deeper understanding of the relevant science; this further prepares the students to conduct their independent research projects at the end of the course.

As one representative example of the weekly structure, we present Week #7, which focuses on foams and emulsions. In lecture, The lab for the week is Mayonnaise and Lime Foam, which shows how the same underlying scientific principles apply to both a traditional and a modernist recipe. Further examples of weekly structures are shown in Fig. B.4.1.

B.4 Week-by-week summary

B.4.1 Energy, Temperature, and Heat

Heating is a universal technique for cooking; the relationship between the heat added Q and the change in temperature ΔT for a mass m of food is $Q = mc_p\Delta T$, where c_p is the specific heat of the food. In lecture, the professors explain how adding cold milk to hot coffee lowers the final temperature.

Lab: Ricotta Cheese

Students prepare cheese by adding an acid to milk, causing it to curdle. As a preview for the following week, they prepare a phase diagram for the effect of vinegar on the physical properties of the milk.

B.4.2 Phases of Matter

The transformations that occur during cooking, such as frying an egg or making ricotta cheese, can be represented on a phase diagram. The raw and cooked states correspond to different regions on the diagram. The boundaries of the phase diagram are determined by where the interaction energy U between molecules in the food is equal to a constant C to the thermal energy k_BT.

Demo: Rotary Evaporator and Pressure Cooker

Pressure is sometimes manipulated by chefs to adjust the cooking process. A common example to show the relationship between pressure and boiling point is

a pressure cooker. Several high-end chefs use rotary evaporators, or rotovaps, to distill flavors from food. By using a reduced pressure, the initial liquid turns into a gas at a temperature below the boiling point at atmospheric pressure, which preserves sensitive aromatic molecules. We show both of these techniques on a phase diagram as a concrete example of the equation of the week.

Demo: Sous-vide cooking

One of the most influential developments in recent years has been sous vide cooking, which allows precise control of the temperature of food. Most proteins, such as eggs, fish, and steak, cook at temperatures far below the boiling point of water. This allows them to be gradually warmed to their ideal temperature in a temperature-controlled water bath.

Homework: Saturated and Unsaturated Fats

Which is stronger, the bond between unsaturated fat molecules or saturated fat molecules? Would having a longer chain length increase or decrease its melting point?

Lab: Ice Cream

Students prepare ice cream using a slurry of salt water and ice to cool the base below 0 °C. They use a phase diagram to explain how the freezing point of water changes with the addition of ice.

B.4.3 Elasticity and Gels

The way that food feels in your mouth, independent of its taste, can be explained in terms of the bonds holding the molecules together. One way to change the texture of food is by adding polymers; the long molecules can stick together to form a continuous network, called a gel. Cheese, such as the ricotta from the first week, is a common example of a gel, made from coagulated proteins in milk.

The texture of a gel, specifically its elasticity E is related to the spacing of bonds between the polymers l by the equation $E = \frac{k_B T}{l^3}$, where $k_B T$ is the thermal energy term introduced in the first week.

Demo: Hydrocolloids in food

Gelatin, such as in Jell-O, is one of the most well-known examples of a gel. Now chefs are experimenting with a wide range of naturally-derived polymers, such as agar and carrageen, to create gels with different textures. A classic application of gels in food is the "Hot and Cold Tea" recipe from Heston Blumenthal, in which the left half of the beverage is hot and right half is cold. The elasticity of a gel is temperature-dependent, so the concentration of the gelling agent in each side is adjusted to match the elasticities, by altering the cross-link spacing l.

Homework: Elasticity of a steak

Elasticity is one way to quantify the doneness of a steak. In class, we measured the elasticity of a medium rare steak as 53 kPa. If you put a 1 kg weight on top of a 4 cm cube of steak, how much would it compress?

Lab: Hot Flan

One hydrocolloid, methycellulose, contrary to nearly all other hydrocolloids, turns into a solid when heated. In the lab, students prepare a hot version of the custard-like dessert, then measure the resulting elasticity E and calculate the cross-link spacing l.

B.4.4 Diffusion

The rate of many culinary processes, such as cooking and brining, is limited by diffusion, in which the distance L traveled by heat or molecules is proportional to the square root of time t: $L = \sqrt{4D\,t}$.

Homework: Searing a steak

Even sous-vide steaks benefit from a quick searing to improve the flavor. To cook just the outer 2 mm of the steak, how long should you sear the steak on each side, assuming a heat diffusion constant of $1.4 \cdot 10^{-3} \text{cm}^2/\text{s}$.

Lab: Spherification

Diffusion and gelation are both essential for a culinary technique called spherification, in which drops of liquid form solid shells around their outsides. One particular implementation, using sodium alginate and calcium, was developed by Ferran Adriá, allowing recipes such as green pea ravioli without any pasta shell or "caviar" made from melon juice. In the lab, students experiment with spherification, and measure the thickness of the solid shell L as a function of time t, in order to calculate the diffusion rate for calcium ions $D_{Ca^{2+}}$.

B.4.5 Heat Transfer

Similar to the ions in the spherificaiton example, thermal energy can flow by diffusion. The rate of this transfer depends on the temperature difference between the temperature of the food T_{in} and the outside T_{out}. The temperature over time $T(t)$ is also related to a time constant τ_0, which depends on the size of the food L and the heat diffusion constant D: $T(t) = (T_{\text{in}} - T_{\text{out}})\, e^{-t/\tau_0} + T_{\text{out}}$ for $\tau_0 = \frac{L_0^2}{4D}$.

Homework: Cooking salmon

How long should we cook a 2" thick salmon steak to reach its ideal temperature of 135 °F? Assume the raw salmon has an initial temperature of 30 °F and a preheated oven is set to 350° F. Note: the diffusion constant of fish is about 10^{-3} cm^2/s.

Lab: Molten Chocolate Cake

In this lab, students use thermocouples to measure the temperature at multiple points within a cake as it bakes. Over the course of about seven minutes, the exterior of the cake sets into a solid, leaving the molten interior. By plotting the thickness L of the solid layer over time, students measure the thermal diffusion constant D of cake batter, which is nearly the same as water.

B.4.6 Viscosity and Polymers

An important aspect of the consistency and mouthfeel of many sauces and beverages is how easily they flow, which is quantified by the viscosity η. At the microscopic level, this property arises from the time-scale for the molecules in a food to move past each other τ_{flow}. Foods that seem viscous over long time-scales can seem highly elastic at short time scales.

Demo: Molecular model with spaghetti

Spaghetti can serve as a model for how the sizes of molecules affect their thickening properties. Long noodles can entangle, so when one noodle is sharply pulled, the network behaves like an elastic solid. However, if a noodle is gently pulled, then it can slide out, like in a viscous liquid.

Lab: Milkshakes

Mass-produced food often uses xanthan gum as a thickening agent. This microbial by-product is so effective since it is an unusually long molecule. In this lab, students vary the amount of xanthan gum in a recipe to match the viscosity of a milk shake, enabling the same consistency with far less fat.

B.4.7 Emulsions and foams

Another way to change the texture of food is by adding droplets or bubbles — the dispersed phase. This is strongly related to the ratio of the volume of droplets

or bubbles to the surrounding liquid, represented by the volume fraction φ. At low concentrations they can thicken a liquid and at high concentrations they can pack together to form a solid. At a critical volume fraction φ_c, the droplets or bubbles cannot be packed any tighter without being deformed, so adding more of the dispersed phase leads to an elastic material.

Demo: Aioli

Aioli is a quintessential condiment from the Catalan region of Spain, made from olive oil, garlic, salt, and a little water. The olive oil forms the dispersed phase of the emulsion, which is stabilized by emulsifiers in the garlic.

Homework: Droplet Size

Two recipes for lactonnaise have the same proportion of oil, but one has been whisked by hand and one with an immersion blender. The droplet size of the hand-whisked emulsion is 100 μm and the droplet size for the blended emulsion is 10 μm. How does the elasticity of the hand-wisked sauce compare to the blended version?

Lab: Mayonnaise and Lime Foam

For the first part of the lab, students prepare some variation of mayonnaise, either with an egg or garlic as an emulsifier, and calculate the volume fraction φ of oil in the resulting emulsion.

Next, they observe the mayonnaise under a microscope at 60x magnification to determine the average radius R of the oil droplets. For the second part of the lab, students prepare a foam from lime juice, using xanthan gum as a stabilizer and measure the size R of the air bubbles at 10x magnification with the microscope.

The students then apply the Equation of the Week, $E = \frac{\sigma}{R}\left(\varphi - \varphi_c\right)$, to explain how the elasticities, E, of these foods are related to the radii, R, of the droplets or bubbles in the dispersed phase, which they just measured. They are

further encouraged to discuss and relate their results to what they have learned about the underlying molecular interactions of emulsifiers and xanthan gum.

B.4.8 Chemical reactions

So far, the course has primarily discussed physical changes in food, which involve the interactions *between* molecules. However, much of the flavor of food is caused by chemical transformation, which involve breaking and reforming the bonds *within* molecules.

Chemical transformations can also transform the physical properties of food, such as leavening in baked goods. Baking soda can react with acids in a dough to produce carbon dioxide bubbles:
$\mathrm{NaHCO_3} + \mathrm{AcidH} \rightarrow \mathrm{AcidNa} + \mathrm{H_2O} + \mathrm{CO_2}$.

Demo: Transglutaminase

Enzymes are molecules that speed up the rate of chemical reactions. One example of this is transglutaminase, which binds together separate protein molecules. Chef Wylie Dufresne (wd-50) has extensively explored its culinary applications, randing from shrimp noodles to radish sheets.

B.4.9 Microbes

Microbes play a profound role in cuisine; most preservation and cooking techniques are ways to kill pathogenic microbes, or at least slow their growth. This is especially important since populations of microbes over time $N(t)$ can grow at an exponential rate: $N(t) = N_0 e^{kt}; k = \ln 2/\tau_2$, for an initial population N_0 and a doubling rate τ_2.

Demo: Fermented Foods

One new frontier in the restaurant world is the use of fermented products. Pork bushi is one example from the Momofuku restaurant group, in which microbes convert pork into a solid, similar to a process used in Japan to make katsuobushi.

Homework: Blue cheese

Suppose that a perfectly-ripened block of blue cheese contains 10^{12} microbes and you have a block with only 1000 microbes. How long do you need to wait for the cheese to ripen, based on a doubling time of 3 hours?

Using both theoretical and practical approaches to teaching physics, we aim to ensure that students gain experience with the scientific concepts from multiple perspectives. In addition, we pursue an iterative approach, framing new material in the context of what was previously presented. For example, during the week on gelation, previous concepts reappear, such as elasticity and diffusion, as shown in Table B.3.1. According to feedback from the teaching staff, many students found this approach helpful for preparing for the exams.

B.5 Assessment of student learning

To assess the extent to which students understand the scientific concepts and methods, we used three main approaches:

1. **Written problem sets**: A weekly problem set, with about five to seven questions, asks qualitative questions about the current concept and quantitative questions about how to apply the Equation of the Week to culinary examples.

2. **Written in-class exams**: A two-hour midterm exam and a three-hour final exam test the abilities of students to integrate scientific concepts from multiple weeks and solve multi-part, quantitative problems. Table B.5.1 provides a representative example of a series of questions that involve chocolate chip cookies, similar to what could appear on a final exam.

3. **Final independent research projects**: The last four weeks of the course are devoted to students working on independent research projects.

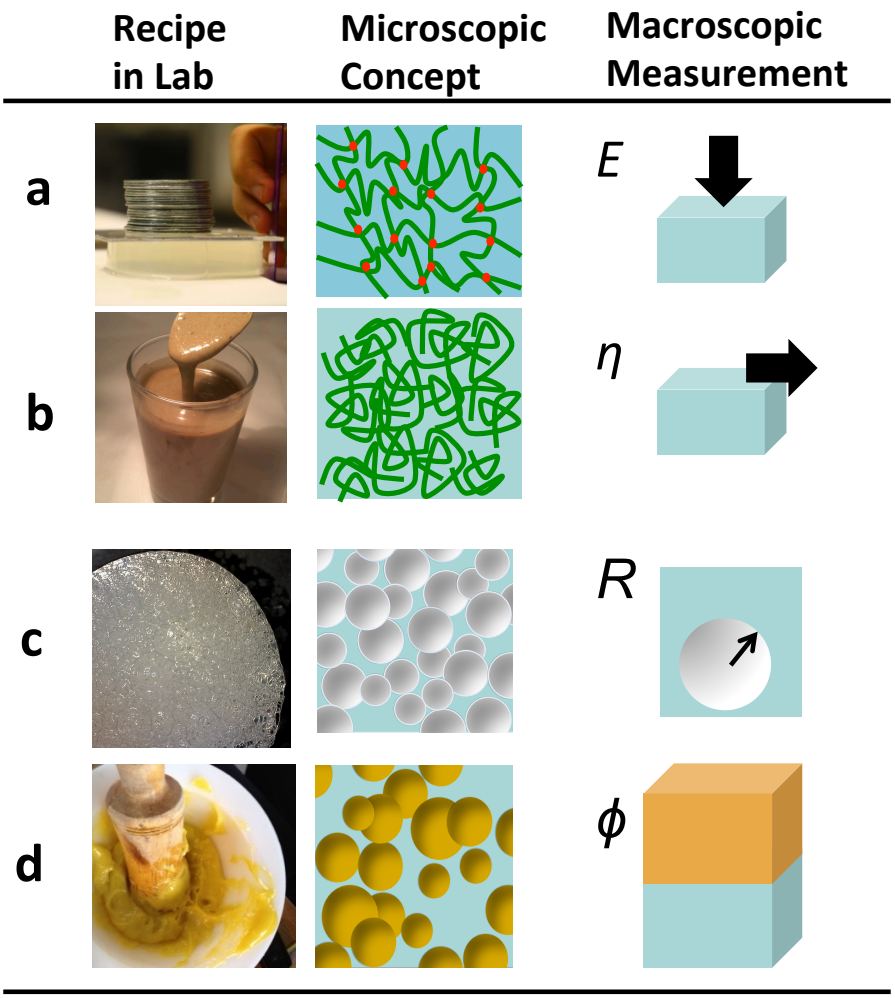

Figure B.4.1: Examples of weekly structure. a) Measure the elasticity, E, of hot flan, a gel made with eggs, and compare to gels made with the polymer gellan at different concentrations. b) Design your own non-melt milkshake by measuring the viscosity, η, as a function of xanthan gum added, and match the viscosity to that of a regular milkshake. c) Design your own culinary foam stabilized by xanthan gum, and measure the volume fraction, φ, of air bubbles; explain elasticity, E, of the foam. d) Measure volume fraction, φ, of oil droplets in aioli, stabilized by garlic or egg yolk lecithin; explain elasticity, E, of the emulsion.

B.6 Final projects

The final projects are one of the most challenging and rewarding aspects of the course for the students. Although we provide them with a list of possible topics,

Table B.5.1: Sample exam problems: Chocolate Chip Cookies

Topic	Question
Elasticity	In an effort to bake chocolate chip cookies of uniform thickness, you decide to use your coffee cup to press the dough. Suppose the cup weighs 100 g. You notice that if you shape the dough initially into a cube 3 x 3 x 3 cm and put the cup on it, the dough compresses to three quarters its original height. What is the elastic modulus of the cookie dough?
Gels	From your calculation of elasticity in the previous problem, calculate the distance between cross-links in the gluten network in the cookie dough, which is the primary determinant of the elastic modulus. Assume the other ingredients do not contribute to the elastic modulus.
Heat transfer	You place the cookies on a pan and bake them in the oven at 375 $^{\circ}$F for 10 minutes. Approximate the dough as a sphere of radius 2 cm and assume that it does not change shape while baking. Also, assume that heat is supplied from all directions. What temperature does the center of each cookie reach?

many of them choose instead to draw on inspiration from the visiting chefs as well as from their own experiences with food to develop their own topics, thus bringing personal creativity and passion to their research. We encourage students to continue refining their ideas in discussion with the chefs and the course staff at all stages of the research process, from brainstorming to data interpretation. We are thus able to create an environment where students are actively engaged to learn the scientific method, while also allowing them creative freedom.

The main criteria of the projects is to address a scientific question related to cooking, then to generate and analyze at least one plot of data that captures the core findings. Students work either alone or in groups of two to three. Each student or group presents their research at a final science fair and submits a final written report. In summarizing several weeks of research in a space-limited format, students are required to practice good skills in science communication, such as choosing which data to present and making their material relevant to their audience [50].

B.6.1 Examples of student final projects

Over the past three years, students have completed hundreds of final projects. Here we discuss a few represetnative examples:

1. **Maillard reaction:** The browning of potatoes depends on a combination of temperature, pH, and time, shown in Fig. B.6.1.

2. **Spherification:** A diffusion-limited gelation process, called spherification, depends on the concentration of ions used to cross-link a polymer, shown in Fig. B.6.2.

3. **Heat resistant chocolate:** The melting point of chocolate increases by adding gelatin and the enzyme transglutaminase, shown in Fig. B.6.3.

B.7 Conclusions

Our experience with these courses demonstrates the potential impact of using examples from the culinary world to teach scientific concepts and methods. The final projects demonstrate the success of this inquiry-based approach in training students to be scientists within an undergraduate course: even non-science majors are able successfully to formulate scientific questions, develop new experimental methods, and analyze and interpret data within a theoretical framework. We also heard several examples of students applying the concepts in their daily lives, such as calculating the cooking time for their Thanksgiving turkey.

Although we conducted the courses at major research institutions with well-known chefs, the same approach could be implemented elsewhere. The lab component could be adapted for any large kitchen, such as a school cafeteria, or as practical homework assignments for the students to complete in their own

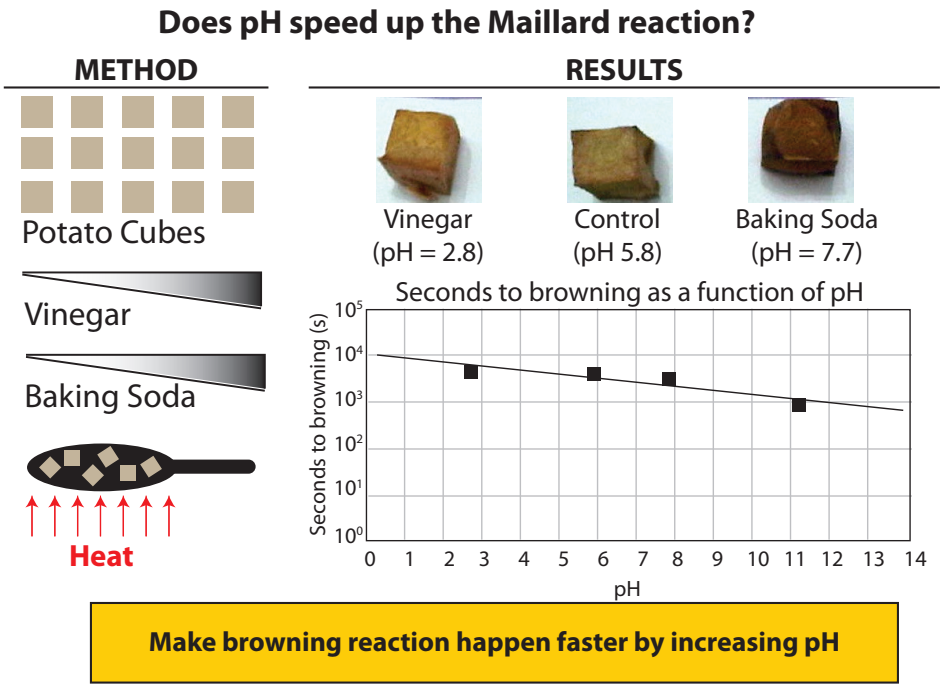

Figure B.6.1: Maillard reaction: Students quantitatively studied the effect of pH on the rate of browning due to the Maillard reaction. The group devised a simple image analysis technique to quantify this process and acquired images of potatoes cooked at different combinations of temperature, pH, and time.

kitchens. Local chefs have a wealth of knowledge about cooking techniques and can serve as mentors for student research projects; we have discovered that chefs are enthusiastic to share their culinary experience with students, and to learn more about the science behind their cuisine. Moreover, utilizing local facilities and culinary talent can more deeply show the connection to the students' everyday lives.

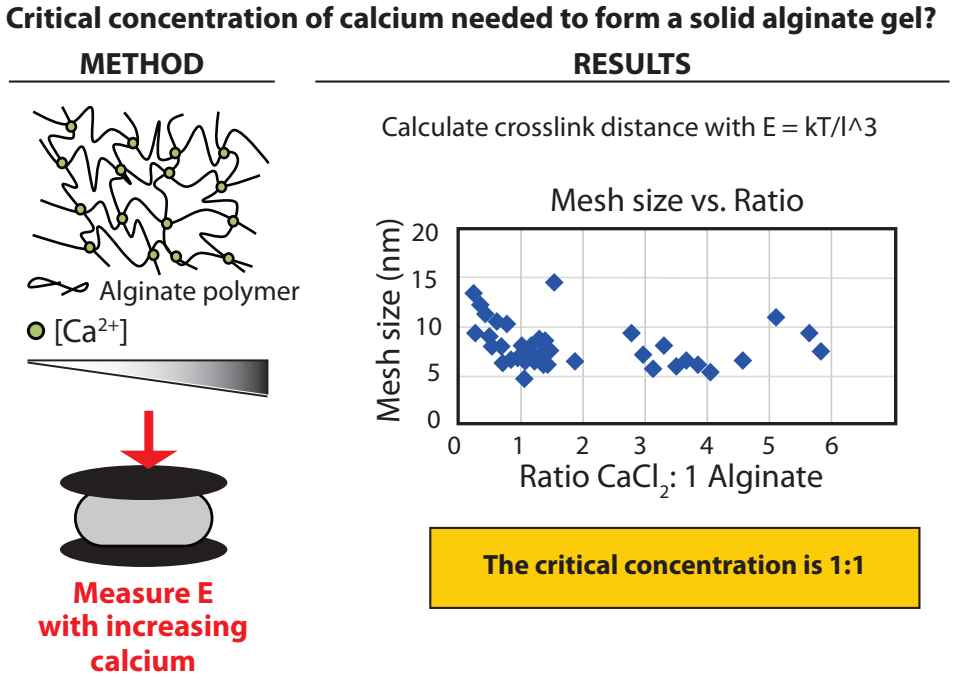

Figure B.6.2: Spherification: Inspired by the visiting chefs who demonstrated the culinary technique known as spherification, a team of students sought to find the critical concentration of calcium required for gelation of an alginate polymer solution. After testing over 60 samples, they discovered that above a molar concentration of 1 calcium ion per 1 alginate molecule, the elasticity of the polymer gel, and therefore the mesh spacing, reached a plateau; this concentration corresponds to the minimum amount of calcium specified in recipes.

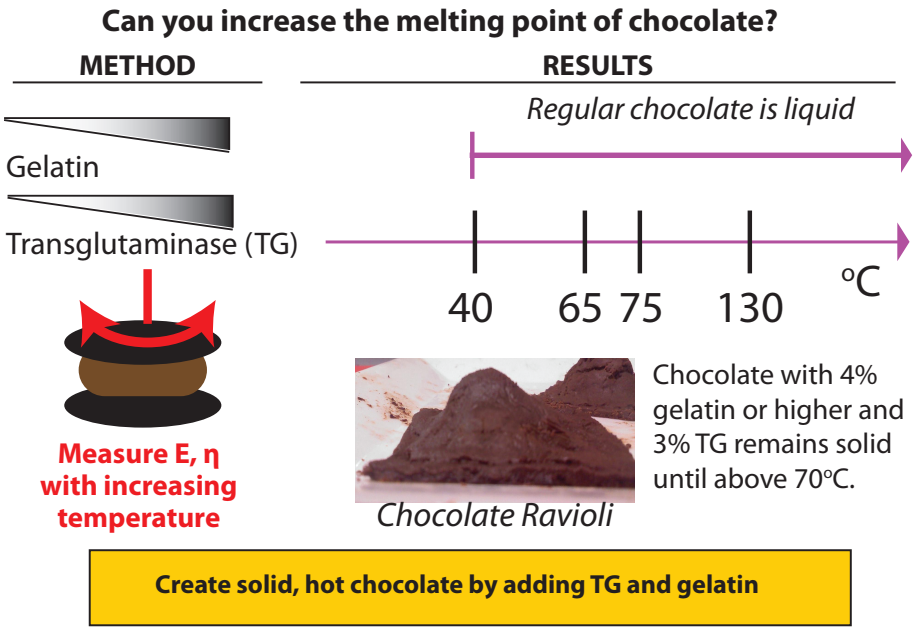

Figure B.6.3: Heat-resistant chocolate: Motivated by chef Wylie Dufresne's lecture, students used the enzyme transglutaminase to create a chocolate composite that retained its solid characteristics even above the normal melting point for dark chocolate. By exploring a range of enzyme and gelatin concentrations, and measuring the elasticity of the final product, the team constructed a phase diagram of chocolate textures.

C

Cocktail Physics

We are in the midst of a culinary revolution, as high-end chefs around the world exploit scientific knowledge and technological advances to create spectacular dishes. Ferran Adrià, for example, known for his world-acclaimed restaurant El Bulli in Catalonia, Spain, has pioneered the use of hydrocolloids to create yogurt spheres, carrot foam, and other novel foods. Other chefs, such as Heston Blumenthal at The Fat Duck in Berkshire, England, Grant Achatz at Alinea, Chicago, and Wylie Dufresne at wd-50, New York, are exploring science-based techniques, including the use of liquid nitrogen, enzymes, and controlled temperature baths to create remarkable juxtapositions of new flavors and unexpected textures.

The same trend is happening, in parallel, with cocktails. For years bartenders have relied on trial and error to refine recipes, but now the same techniques that fueled the culinary revolution are allowing a more systematic approach to

developing new drinks. Tools and techniques borrowed from research laboratories in physics and chemistry, such as rotary evaporators, thermocouples and centrifuges, are helping bartenders to better realize their fantastical innovative drinks ideas. Concepts from thermodynamics as well as the physics of colloids, gels and other forms of "soft matter"can help explain the flavor, appearance, and "mouthfeel" of these beverages.

C.1 Full of flavor

Be it in beer, wine, vodka, or a martini, the physical properties of ethanol, especially its solubility and volatility, facilitate the delivery of flavors impossible to achieve using water alone. What we think of as "flavor" actually has two main components: its taste and its aroma. As food-science author Harold McGee puts it, "tastes provide the foundation of flavor, and aromas provide the tremendous variety." We can perceive five basic tastes on the tongue (sweet, sour, salty, bitter and savoury) but there are thousands of aromas that we can sense through olfactory receptors in the nose – be it the caramel notes of rum or the oaky smell of bourbon.

Alcohol is far more effective than water at delivering these aromatic components, since they are typically not especially water-soluble. Water molecules, in contrast, are polar and so prefer to be near other polar molecules to minimize their interaction energy. This encourages non-polar molecules, like the aromatics, to leave the liquid phase and vaporize into the surrounding air, where they contribute to the gaseous aroma of the drink. The presence of ethanol mediates this polar/non-polar interaction and allows high concentrations of aromatics to remain in an aqueous solution. For this reason, ethanol is used to extract and deliver flavors from a range of sources, including flowers, spices, nuts, fruits, and herbs.

Distilled alcoholic liquids, called spirits, are the essential component of any cocktail. Naturally fermented alcoholic beverages, such as beer and wine, rarely exceed about 20% ethanol by volume, since higher levels are toxic to the yeast

that produce it. Therefore, higher concentrations must be reached through distillation, in which the fermented beverage is heated to preferentially extract the ethanol, which has a lower boiling point than water. The plant material used during fermentation, such as molasses for rum or agave for tequila, gives an intense flavor to the final distilled beverage. Additional plant material supplied during or after distillation, such as the juniper berries used for making gin, also contribute to the flavor. Due to the high concentration of aromatic molecules extracted from the plants during the production process, spirits are some of the most intensely flavored foods. Indeed, only a few drops of Chartreuse, a French liqueur made from nearly 130 herbal extracts, can entirely change a cocktail's flavor.

Distillation has been used for thousands of years to create spirits, going as far back as Mesopotamia and ancient China, but continues to be improved through applications of scientific knowledge. For example, some bartenders, such as award-winner Tony Conigliaro of London bar 69 Colebrooke Row [51], are experimenting with a device commonly found in the science lab, known as a rotary evaporator, shown in Fig. C.1.1. This device extracts aroma molecules that would otherwise be destroyed by the higher temperatures in traditional distillation techniques. The rotary evaporator lowers the pressure inside a rotating container holding the liquid to be distilled, causing the more volatile components to evaporate, and leaving behind the undesirable water, sugar, pigments, and other large molecules. A condensing coil uses a coolant to turn the vapors back into a liquid – the final intensely-flavored product – which is collected in a separate flask. A habañero liqueur is one illustrative example: the capsaicin that makes the chili intensely hot is non-volatile, so only the fruity and floral compounds end up in the distillate, yielding a liqueur that retains all the flavor of the chilies without any nasty burn.

Another way to intensely flavor spirits is to soak ingredients in high concentrations of ethanol, thereby infusing the aromatics into the alcohol. This process traditionally requires many days for the ethanol to fully penetrate the

Figure C.1.1: Diagram of a rotary evaporator. The liquid in the rotating chamber (red) is gently heated while put under a vacuum, causing it to vaporize at a lower temperature. The condenser coils (blue) liquefy the vapor, which is collected in the flask on the left (green). Photo credits: Dave Arnold, cookingissues.com

ingredients and extract the desired compounds. Now, however, flavor infusion can be achieved in just a few minutes, using a technique pioneered by Dave Arnold, director of culinary technology at The French Culinary Institute in the US. Coffee-flavored vodka, for example, can be made by combining ground coffee beans and vodka along with nitrous oxide in a whipped cream dispenser – a pressurized device typically used to create thick cream foams like whipped cream at the touch of a button, now well known by the commercial name iSi whip. For the coffee-flavored vodka, the nitrous oxide, which is under pressure in the canister, dissolves in the vodka. The high pressure of the liquid displaces any air bubbles in the coffee grounds. When the pressure is released, the nitrous oxide rapidly bubbles out of solution, just like what happens when opening a can of carbonated drink. Releasing these bubbles draws flavor molecules from the coffee grounds into the vodka, flavoring the alcohol and turning it brown. This versatile technique works for a range of porous substances, such as cocoa nibs and a variety of herbs.

By combining the spirits with other ingredients, a full spectrum of flavors can

be achieved. Tastes can be added through the sweetness of syrups, the sourness of citrus juice, the salt around the rim of a glass, or numerous other methods. Aromas can be enhanced with a variety of highly concentrated alcohol-based solutions called liqueurs, tinctures, and bitters. In beer and wine, as opposed to mixed drinks, there is less flexibility in what can be produced because flavors are limited and are dictated by the compounds present in the initial grains or fruits used as the carbohydrate sources for fermentation.

C.2 Hot or cold

Whether by dare or choice, many have experienced the hot, burning sensation from drinking straight vodka or tequila. In cocktails this can overwhelm the desired mix of flavors. But the alcohol burn can, however, be reduced by lowering the temperature of the beverage, which is why aquavit, vodka, and other straight spirits are often served cold, at temperatures around −18°C. Unfortunately such low temperatures also diminish the perception of the other tastes and aromas in the drinks, so most mixed drinks are served at somewhat warmer temperatures.

The flavor of a drink also depends on how diluted it is, which in practical terms means how much ice has been mixed in it. Vigorously shaking the mixture rapidly cools the drink within seconds, whereas cooling can take upwards of a few minutes if it is only gently stirred [52]. In both cases, the final temperature of the diluted mixture can be several degrees below the initial temperature of the ice, for essentially the same reason that roads are de-iced by spreading salt on them. Because the entropy of the diluted mixture is far larger than the entropy of the crystalline ice, the ice continues to melt and absorb heat from the mixture even as the mixture cools below 0°C.

The precise temperature of the drink also strongly affects the complex balance between these flavors. A chilled martini, for example, is crisp and balanced, whereas gin can overwhelm the flavor near room temperature. As McGee explains, "the bartender's challenge is to make drinks that have a balanced taste foundation and aromas that suit that foundation, and retain that overall structure

reasonably well over the drink's lifetime, as it becomes diluted or warms up."

C.3 Look and feel

The flavor of a cocktail is of course important but its appearance and texture also contribute to the overall experience of the drink – be the layers of a squashed frog, a creamy snowball, the creaminess of egg nog, or even a Blue Blazer, which is poured between two cups after being set on fire. Flames and decorations aside, a cocktail's appearance results from a combination of its color and opacity, both of which can be controlled by the bartender. For a colored drink, the bartender selects ingredients that absorb specific wavelengths. For example, a rich brown can be obtained using a spirit that has been aged in oak barrels as this imparts pigment molecules that produce this color. If you want the finished drink to be clear, all the pigments and particulates must be removed, then obviously each of its components must also be clear, to prevent light absorption or scattering.

But even with clarified components, the mixing technique can have a dramatic impact on the light-scattering properties of the finished drink. For example, a Manhattan, which contains whiskey, vermouth and bitters, can become cloudy when shaken. This results from small air bubbles introduced into the beverage while shaking, which are then stabilized by the bitters. A stirred Manhattan, in contrast, is clear, as shown in Fig. C.3.1.

As for drinks that are cloudy, their appearance is often caused by the presence of small particulates, although these can be removed by a variety of clarification techniques. Surprisingly, the most common method of clarification, filtration, is rarely used. Instead, some bartenders with an interest in molecular gastronomy are turning to other techniques such as centrifugation, which rapidly produces a clear liquid by accelerating the settling of particulates. Indeed, this technique is a particularly good way of clarifying lime juice, which can then be used for transparent gin and tonics or clear, stirred margaritas. Another technique, also developed by Arnold, uses gels made from agar – a naturally occurring

Figure C.3.1: Shaken and stirred Manhattan: The shaken martini (left) has a froth on the surface and cloudy appearance, due to vigorous shaking causing incorporation of air bubbles, while the stirred martini (right) is clear. Photo credits: Mike Betancourt and Leo Stein

polysaccharide – to trap particulates from citrus juices and other non-transparent liquids. Water is boiled with agar to hydrate it, the juice is then added and the solution is allowed to cool to form a gel. The longer pectin fibers and other plant materials become trapped in the agar gel, and a clear liquid weeps out, which also contains the much smaller flavor molecules.

There is also plenty of interesting physics going on in drinks that include anise-flavored spirits like pastis, ouzo and absinthe. These contain water-insoluble anethole compounds, like the anethole molecules found in drinks containing extracts from anise, caraway, and similar plants in the carrot family. As described earlier, the anethole dissolves in ethanol, due to the alcohol's unique structure. But, when diluted with water, these compounds are no longer soluble. They form a spontaneous emulsion, a highly concentrated suspension of microscopic droplets, that strongly scatters light. Because of the small size of the droplets, these emulsions are stable for months, without the addition of any additional surfactant [53]. This effect is exemplified in a drink called Half sinner, half saint. A layer of pastis is floated on top of a mixture of sweet and dry vermouth. The pastis spreads downwards, leading to a white layer, caused by the droplets of anethole that travel from the top to the bottom of the glass over the

Figure C.3.2: Half sinner, half saint. Before the pastis is added (left), the drink is clear. After the pastis is added (middle), the top of the drink becomes cloudy as a spontaneous emulsion of the oils in the pastis is formed. After several minutes (right), the emulsion drops spread halfway down the glass, producing an opaque white layer. Photo credits: Mike Betancourt and Leo Stein

course of several minutes, as shown in the time series of Fig. C.3.2.

In addition to flavour and appearance, the "mouthfeel" of a drink is another parameter manipulated by bartenders. Incorporating air via shaking also results in a more viscous texture. Egg whites are used in fizzes and sours to stabilize these air bubbles. An extreme example is a Ramos Gin Fizz, which calls for an exhausting 12 minutes of shaking in the original recipe. The effort is worth it, however, as it results in an extremely creamy, frothy texture, as shown in Fig. C.3.3. A layer of foam protrudes several centimeters above the rim of the glass and is stiff enough to hold a metal straw vertically down the center. The long mixing time is needed to divide the air into progressively smaller bubbles, resulting in a stiffer foam. Another class of drinks, called flips, uses the whole egg to form an emulsion, leading to a more creamy texture.

Several of the chefs leading the innovations in haute cuisine are also pushing the frontiers of texture in a cocktail. Ferran Adriá served several novel types of cocktail in his restaurant, including a hot and cold gin fizz (see C.4). Instead of the lengthy shaking of the Ramos Gin Fizz, an iSi whip introduces nitrous oxide bubbles into the top foam layer, which sits on top of a frozen cream layer. At Grant Acahtz' Aviary, the cocktail chefs use techniques developed in the Alinea kitchen to create novel forms for the drinks. For instance, they use a modified

Figure C.3.3: Ramos gin fizz. The egg whites and cream in the drink stabilize a thick layer of foam, which extends beyond the top of the glass and can support a metal spoon. Photo credits: Aaron Rosenthal

starch called tapioca maltodextrin to produce a powdered gin and tonic or ultra-low temperatures to make chewy Pisco sour. Other mixologists, such as Eben Freeman, use similar techniques to create a variety of solid cocktails.

These elements of flavor, appearance, and texture all contribute to the final perception of the drink. Classic cocktail recipes have survived and evolved with improvement of their balance of these components. Bartenders today are using tools from science to better present classic recipes and to invent new concoctions. The art of mixology lies in balancing flavors and satisfying personal preferences. Tools from science can help achieve this goal.

C.4 Recipes

Here are some cocktail recipes you can try for yourself, from two leaders in the field, who have rather different approaches to cocktails. some of the leaders in the molecular gastronomy of cocktails.

C.4.1 Hot and cold gin fizz

Ferran Adrià, el Bulli

Ingredients

Table C.4.1: Ingredients

For the syrup base:		
150	g	sugar
150	g	water
For the frozen lemon juice:		
250	g	lemon juice
150	g	syrup base (see above)
150	g	gin
For the hot lemon foam:		
150	g	egg whites
130	g	lemon juice
70	g	gin
145	g	base syrup (see above)
1/2	liter	iSi Whip
1	cartridge	N2O

Procedure

For the syrup base: Mix both ingredients and bring to a boil. Remove from heat, let cool and refrigerate. **For the frozen lemon cream:** Mix all ingredients

and put in freezer. Once frozen, blend in the blender until fluid. Store in the freezer. **For the hot lemon foam:** Break the egg whites with a whisk. Add the remaining ingredients. Strain and pour into the iSi with the help of a funnel. Load the iSi and keep in a water bath at 80°C. Swirl from time to time.

Serving

Fill 3/4 of a cocktail glass with frozen lemon juice. Top the cup with hot foam.

C.4.2 Half sinner, half saint

John Gertsen, bar manager at Drink, Boston

Ingredients

Table C.4.2: Ingredients

2	oz	sweet vermouth
2	oz	dry vermouth
1	barspoon	pastis

Procedure

In a rocks glass with ice, pour both vermouths and mix. Float the pastis on top.

Biofilm References

[1] H. Vlamakis, Y. Chai, P. Beauregard, R. Losick, and R. Kolter, **11**, 157–168 (2013).

[2] L. Hall-Stoodley, J. W. Costerton, and P. Stoodley, **2**, 95–108 (2004).

[3] *Household biofilms* (2006), URL http://www.biofilm.montana.edu/content/household-biofilms.

[4] S. R. Gill, **312**, 1355–1359 (2006).

[5] A. M. Valm, J. L. M. Welch, C. W. Rieken, Y. Hasegawa, M. L. Sogin, R. Oldenbourg, F. E. Dewhirst, and G. G. Borisy, **108**, 4152–4157 (2011).

[6] L. Hall-Stoodley and P. Stoodley, **11**, 1034–1043 (2009).

[7] K. Lewis, **64**, 357–372 (2010).

[8] R. Singh, D. Paul, and R. K. Jain, **14**, 389–397 (2006).

[9] E. J. Gardel, M. E. Nielsen, P. T. Grisdela, Jr., and P. R. Girguis, **46**, 5222–5229 (2012).

[10] A. E. Franks, N. Malvankar, and K. P. Nevin, **1**, 589–604 (2010).

[11] K. Drescher, Y. Shen, B. L. Bassler, and H. A. Stone, **110**, 4345–4350 (2013).

[12] D. Lopez, H. Vlamakis, and R. Kolter, **33**, 152–163 (2009).

[13] D. López and R. Kolter, **34**, 134–149 (2010).

[14] I. G. de Jong, J.-W. Veening, and O. P. Kuipers, **14**, 3110–3121 (2012).

[15] J.-W. Veening, E. J. Stewart, T. W. Berngruber, F. Taddei, O. P. Kuipers, and L. W. Hamoen, **105**, 4393–4398 (2008).

[16] J. C. W. Locke and M. B. Elowitz, **7**, 383–392 (2009).

[17] G. O'Toole, H. B. Kaplan, and R. Kolter, **54**, 49–79 (2000).

[18] M. Perego, C. F. Higgins, S. R. Pearce, M. P. Gallagher, and J. A. Hoch, **5**, 173–185 (1991), ISSN 1365-2958, URL http://dx.doi.org/10.1111/j.1365-2958.1991.tb01838.x.

[19] P. Eswaramoorthy, J. Dinh, D. Duan, O. A. Igoshin, and M. Fujita, **156**, 2294–2304 (2010).

[20] I. Kolodkin-Gal, A. K. W. Elsholz, C. Muth, P. R. Girguis, R. Kolter, and R. Losick, **27**, 887–899 (2013).

[21] M. Shemesh and Y. Chai, **195**, 2747–2754 (2013).

[22] S. M. Rubinstein, I. Kolodkin-Gal, A. Mcloon, L. Chai, R. Kolter, R. Losick, and D. A. Weitz, **86**, 426–436 (2012).

[23] C. Aguilar, H. Vlamakis, A. Guzman, R. Losick, and R. Kolter, **1**, e00035–10–e00035–10 (2010).

[24] Y. Chen, S. Cao, Y. Chai, J. Clardy, R. Kolter, J.-h. Guo, and R. Losick, **85**, 418–430 (2012).

[25] E. A. Shank and R. Kolter, **14**, 741–747 (2011).

[26] A. L. McLoon, I. Kolodkin-Gal, S. M. Rubinstein, R. Kolter, and R. Losick, **193**, 679–685 (2011).

[27] H. Vlamakis, C. Aguilar, R. Losick, and R. Kolter, **22**, 945–953 (2008).

[28] J. Sambrook, D. W. Russell, and D. W. Russell (2001).

[29] S. Chang and S. N. Cohen, **168**, 111–115 (1979).

[30] R. E. Yasbin and F. E. Young, **14**, 1343–1348 (1974).

[31] D. B. Mirel and M. J. Chamberlin, **171**, 3095–3101 (1989).

[32] R. Terra, N. R. Stanley-Wall, G. Cao, and B. A. Lazazzera, **194**, 2781–2790 (2012).

[33] S. S. Branda, J. E. González-Pastor, S. Ben-Yehuda, R. Losick, and R. Kolter, **98**, 11621–11626 (2001).

[34] M. Asally, M. Kittisopikul, P. Rué, Y. Du, Z. Hu, T. \cCa\ugatay, A. B. Robinson, H. Lu, J. Garcia-Ojalvo, and G. M. Süel, **109**, 18891–18896 (2012).

[35] T. A. Barnett, D. Valenzuela, S. Riner, and J. H. Hageman, **29**, 96–101 (1983).

[36] A. Seminara, T. E. Angelini, J. N. Wilking, H. Vlamakis, S. Ebrahim, R. Kolter, D. A. Weitz, and M. P. Brenner, **109**, 1116–1121 (2012).

[37] J. N. Wilking, T. E. Angelini, A. Seminara, M. P. Brenner, and D. A. Weitz, **36**, 385–391 (2011).

[38] K. Kovárová-Kovar and T. Egli, **62**, 646–666 (1998).

[39] I. G. de Jong, K. Beilharz, O. P. Kuipers, and J.-W. Veening (2011).

Science and Cooking References

[40] E. A. Olszewski, **74**, 502 (2006).

[41] C. Vega, J. Ubbink, and E. Van der Lindern, eds., *The Kitchen as Laboratory* (Columbia University Press, 2012).

[42] F. Adria, *Molecular Gastronomy: A to Z* (CRC Press, elBullitaller, 2009), 1st ed.

[43] N. Myhrvold and R. M. Smith, *Modernist cuisine* (Taschen, 2011).

[44] J. Roca and S. Brugus, *Sous-Vide Cuisine* (Montagud Editores, 2005).

[45] S. J. Schmidt, D. M. Bohn, A. J. Rasmussen, and E. A. Sutherland, **11**, 16–22 (2012).

[46] D. T. M. Bachman and J. K, p. 1–5 (2009).

[47] H. McGee, J. McInerney, and A. Harrus, **52**, 30 (1999).

[48] R. M. Felder and L. K. Silverman, **78**, 674–681 (1988).

[49] M. A. Park Rogers and S. K. Abell, **92**, 591–607 (2008).

[50] C. Moskovitz and D. Kellogg, **332**, 919–920 (2011).

Cocktail Physics References

[51] I. Cameron, *In the lab with tony c* (2013), URL http://www.diffordsguide.com/class-magazine/read-online/en/2012-02-21/page-5/inside-tonys-lab.

[52] D. Arnold, *Cocktail science in general: Part 1 of 2* (2010), URL http://www.cookingissues.com/2010/09/02/cocktail-science-in-general-part-1-of-2/.

[53] N. L. Sitnikova, R. Sprik, G. Wegdam, and E. Eiser, **21**, 7083–7089 (2005).

Colophon

This thesis was typeset using LaTeX, originally developed by Leslie Lamport and based on Donald Knuth's TeX. The body text is set in 11 point Arno Pro, designed by Robert Slimbach in the style of book types from the Aldine Press in Venice, and issued by Adobe in 2007. A template, which can be used to format a PhD thesis with this look and feel, has been released under the permissive MIT (X11) license, and can be found online at github.com/suchow/ or from the author at suchow@post.harvard.edu.